

Strong Electroweak Phase Transitions in the Standard Model with a Singlet

J.R. Espinosa^{a,b}, T. Konstandin^c and F. Riva^b

^a*ICREA, Institució Catalana de Recerca i Estudis Avançats,*

^b*IFAE, Universitat Autònoma de Barcelona, 08193 Bellaterra, Barcelona, Spain*

^c*Physics Department, CERN, CH-1211 Geneva 23, Switzerland*

Abstract

It is well known that the electroweak phase transition (EWPhT) in extensions of the Standard Model with one real scalar singlet can be first-order for realistic values of the Higgs mass. We revisit this scenario with the most general renormalizable scalar potential systematically identifying all regions in parameter space that develop, due to tree-level dynamics, a potential barrier at the critical temperature that is strong enough to avoid sphaleron wash-out of the baryon asymmetry. Such strong EWPhTs allow for a simple mean-field approximation and an analytic treatment of the free-energy that leads to very good theoretical control and understanding of the different mechanisms that can make the transition strong. We identify a new realization of such mechanism, based on a flat direction developing at the critical temperature, which could operate in other models. Finally, we discuss in detail some special cases of the model performing a numerical calculation of the one-loop free-energy that improves over the mean-field approximation and confirms the analytical expectations.

1 Introduction

The search for physics beyond the Standard Model (SM) has strong theoretical and experimental motivation and the simplest extension is to enhance the SM by a scalar gauge singlet degree of freedom. This minimalistic model (and its cousins with a complex singlet or supersymmetric versions of it) can be very successful in explaining various phenomena that cannot be explained by the SM: dark matter [1]-[8], spontaneous $B - L$ breaking [9]-[14] and the baryon asymmetry of the Universe [15, 16], often leading to characteristic collider signatures [17]-[23].

One prominent difference between the SM and its singlet extensions is the following. While in the SM the LEP bound on the Higgs mass ($M_h > 114.4$ GeV [24]) implies that the electroweak phase transition (EWPhT) is not first-order but a smooth crossover [25], the addition of a singlet can lead to strongly first-order EWPhTs [26]-[42] for realistic values of the scalar masses. Moreover, with such strong EWPhTs, not only the observed baryon asymmetry of the Universe can be explained through electroweak (EW) baryogenesis (provided the model also contains additional sources of CP violation) but the process of EW symmetry breaking can also leave the trace of a stochastic background of gravitational waves [43].

The aim of the present work is to revisit the EWPhT in the most general renormalizable extension of the SM with one additional real scalar singlet. Although this issue has been studied in the past [26]-[42], (both numerically and analytically at different levels of generality), we believe that a thorough *analytical* understanding of the rich spectrum of possibilities for a strong EWPhT this model offers is still lacking in the literature. The analysis that comes closest to this task is Ref. [35], over which we will improve in a number of aspects.

In the SM and some extensions of it, a first-order EWPhT is caused by the thermal effects of bosons coupled to the Higgs, that generate a cubic term in the Higgs scalar potential. Although this can be successful in many cases, it requires sizeable couplings of these bosons to the Higgs and the effect can be screened by thermal masses when daisy resummation is taken into account. In this article, we concentrate on EWPhTs for which the barrier separating broken and symmetric vacua is not generated by the previous thermal cubic correction but rather by tree-level effects. These tree-level effects lead in general to stronger EWPhTs as $v_c = v(T_c)$, the Higgs vacuum expectation value (VEV) at the critical temperature T_c (that controls through the celebrated ratio v_c/T_c the sphaleron erasure of the baryon asymmetry), is now proportional to some T -independent dimensionful parameter in the potential; hence v_c/T_c can become potentially very large for small T_c .¹ The parameter space of this model

¹Strong EWPhTs are particularly welcome if, as suggested by [36], magnetic fields generated at the

is quite rich and we will see that these tree-level barriers are not necessarily related to the presence of cubic terms in the potential, as is often assumed.

We begin in Section 2 by studying the structure of the tree-level scalar potential of the model. In particular we are interested in potentials where the EW breaking and preserving minima are degenerate, since this is the situation that arises for strong phase transitions. Indeed, in this case it is well justified to use the mean-field approximation for the free-energy, which will have the same structure as the tree-level potential (with temperature-dependent parameters). Differently from previous analyses, we will introduce a novel set of parameters particularly convenient for the discussion of the vacuum structure of this kind of potentials (and which might also be of use for phenomenological studies of the scalar sector of these models). In spite of the large number of free parameters (eight) we have to deal with, this new parametrization will allow us to identify very easily, and analytically, the structure of the potential: its stable minima and the existence of a barrier between them. As a result, beside developing a better understanding of the ingredients necessary to get a strong EWPhT in this model, we will find new scenarios with strong EWPhTs that had not been identified before (involving in particular flat directions at the critical temperature).

In Section 3 we discuss thermal corrections to the scalar potential and explain our strategy to search for regions in parameter space with strong EWPhTs, which we summarize in Table 1. The idea is to start from a potential with degenerate broken and unbroken minima and a barrier between them: this is identified with a potential at T_c which gives a strong EWPhT. Its parameters are then evolved to lower T to find their values at $T = 0$, where they can be used for phenomenological purposes. After identifying the regions in parameter space that give a strong EWPhT, we then perform a more precise analysis including one-loop corrections (at $T = 0$ and finite temperature) without resorting to high- T expansions and including daisy resummation. Although the strength of the EWPhT is somewhat reduced with respect to tree-level, one still gets sizable values for it. Our results confirm then the expectations based on the tree-level analysis.

In the rest of the paper we apply these tools to particular realizations of the model previously considered in the literature: the \mathbf{Z}_2 -symmetric case in Section 4; a particular supersymmetric incarnation in Section 5; and a case with a very light scalar in Section 6. Finally, we study some examples of the general case in Section 7 and conclude in Section 8. Appendix A contains some technical details of the full one-loop analysis, including the $T = 0$ renormalization conditions.

EWPhT lower the sphaleron energy so that larger values of v_c/T_c are required to avoid baryon washout.

2 Tree-level Scalar Potential

2.1 Parametrization of the Potential

To begin with, we look for a convenient parametrization of the potential that ensures control over its minima: this will allow us to easily identify which are the global minima and whether or not they are stable. The most general (renormalizable) tree-level potential for the SM Higgs field h and the singlet s depends on 8 parameters,

$$V = -\frac{1}{2}\mu_h^2 h^2 + \frac{1}{4}\lambda_h h^4 + \frac{1}{2}\mu_s^2 s^2 + \frac{1}{4}\lambda_s s^4 + \frac{1}{4}\mu_m s h^2 + \frac{1}{4}\lambda_m s^2 h^2 + \mu_1^3 s + \frac{1}{3}\mu_3 s^3 . \quad (2.1)$$

Note that a redefinition of the singlet field by a constant shift, $s \rightarrow s + \sigma$, simply amounts to a redefinition of the parameters $\mu_1^3, \mu_s^2, \mu_h^2, \mu_3$ and μ_m but does not change the physics, being just a coordinate change:

$$\begin{aligned} \mu_1^3 &\rightarrow \mu_1^3 + \lambda_s \sigma^3 + \mu_3 \sigma^2 + \mu_s^2 \sigma , \\ \mu_s^2 &\rightarrow \mu_s^2 + 3\lambda_s \sigma^2 + 2\mu_3 \sigma , \\ \mu_h^2 &\rightarrow \mu_h^2 - \frac{1}{2}\lambda_m \sigma^2 - \frac{1}{2}\mu_m \sigma , \\ \mu_3 &\rightarrow \mu_3 + 3\lambda_s \sigma , \\ \mu_m &\rightarrow \mu_m + 2\lambda_m \sigma . \end{aligned} \quad (2.2)$$

This shift is often used to get rid of one of the initial parameters, choosing e.g. $\mu_1 = 0$ or $\mu_3 = 0$.² However, different choices can be useful in different circumstances so we refrain from any particular choice at this stage and keep the discussion as general as possible. Still, it is of advantage to choose a parametrization in which the shift symmetry is realized in a more explicit way. Beside this property, the new parameters will allow for a more direct theoretical control of the structure of the potential. The parameters we introduce are: the vacuum expectation values $v \equiv \langle h \rangle$ and $w \equiv \langle s \rangle$ in the broken minimum; the three elements of the scalar squared-mass matrix, evaluated at the broken minimum (as indicated by the subscript b),

$$m_h^2 \equiv \left. \frac{\partial^2 V}{\partial h \partial h} \right|_b , \quad m_s^2 \equiv \left. \frac{\partial^2 V}{\partial s \partial s} \right|_b , \quad m_{sh}^2 \equiv \left. \frac{\partial^2 V}{\partial h \partial s} \right|_b ; \quad (2.3)$$

the mixed quartic coupling λ_m ; the effective coupling λ^2 defined by

$$\lambda^2 \equiv \lambda_h \lambda_s - \frac{1}{4}\lambda_m^2 , \quad (2.4)$$

²If the potential is invariant under the discrete \mathbf{Z}_2 symmetry $s \rightarrow -s$ then $\mu_m = \mu_1 = \mu_3 = 0$ is the best "coordinate frame" for the singlet as it makes explicitly apparent such symmetry.

that appears recurrently in different contexts (note that λ^2 can be negative); and finally, the combination

$$m_* = \lambda^2 w + \frac{1}{3} \lambda_h \mu_3 - \frac{1}{8} \lambda_m \mu_m , \quad (2.5)$$

which can be checked to be shift-invariant.

To sum up, our parameters are

$$\{v, w, m_h^2, m_s^2, m_{sh}^2, \lambda_m, \lambda^2, m_*\} . \quad (2.6)$$

With the exception of w (transforming as $w \rightarrow w - \sigma$), all these parameters are shift-independent. For reasons that will become clear when we discuss the thermal potential, it is convenient not to assume at this point that v takes its standard value $v_{EW} = 246$ GeV. To avoid confusion later on, we reserve the notation v_{EW} for the latter value. The relations between the old and the new parameters are:

$$\mu_h^2 = \frac{1}{2} m_h^2 + \frac{w}{v} m_{sh}^2 - \frac{1}{2} \lambda_m w^2 , \quad (2.7)$$

$$\mu_s^2 = m_s^2 - \frac{1}{2} \lambda_m v^2 + \frac{3vw}{2m_h^2} [-2\lambda_m m_{sh}^2 - 8m_* v + (4\lambda^2 + \lambda_m^2)vw] , \quad (2.8)$$

$$\mu_3 = \frac{3v}{2m_h^2} [4m_* v + \lambda_m m_{sh}^2 - (4\lambda^2 + \lambda_m^2)vw] , \quad (2.9)$$

$$\mu_m = 2 \frac{m_{sh}^2}{v} - 2\lambda_m w , \quad (2.10)$$

$$\mu_1^3 = \frac{v}{2} (\lambda_m v w - m_{sh}^2) - m_s^2 w + \frac{vw^2}{2m_h^2} [3\lambda_m m_{sh}^2 + 12m_* v - (4\lambda^2 + \lambda_m^2)vw] , \quad (2.11)$$

$$\lambda_h = \frac{1}{2} \frac{m_h^2}{v^2} , \quad (2.12)$$

$$\lambda_s = (4\lambda^2 + \lambda_m^2) \frac{v^2}{2m_h^2} . \quad (2.13)$$

This change of variables is non-singular: indeed its Jacobian is simply $12(m_s^2 m_h^2 - m_{sh}^4)/m_h^4$ which, as shown in the next Section [eq. (2.15)], is always positive and non-singular.

The potential in the new parametrization reads (up to an appropriate constant)

$$\begin{aligned} V &= \frac{m_h^2}{8v^2} (h^2 - v^2)^2 + \frac{m_{sh}^2}{2v} (h^2 - v^2) (s - w) + \frac{1}{4} [2m_s^2 + \lambda_m (h^2 - v^2)] (s - w)^2 \\ &+ \frac{1}{2m_h^2} (\lambda_m m_{sh}^2 + 4m_* v) v (s - w)^3 + \frac{1}{8m_h^2} (4\lambda^2 + \lambda_m^2) v^2 (s - w)^4 , \end{aligned} \quad (2.14)$$

where we have expressed it as a polynomial in $(s - w)$, showing explicitly that now the parameter w can be used to absorb any shift in s , leaving the other parameters of the potential invariant.

2.2 Structure of the Potential

As a good starting point for the analysis, we would like our tree-level potential to be well-behaved. First, it should have a stable broken-phase minimum (v, w) . This is guaranteed by using v and w as input parameters and by a judicious choice of the mass-matrix elements in (2.3), such that both mass eigenvalues are real and positive, that is,

$$\text{Det } \mathcal{M}_s^2 = m_{s_1}^2 m_{s_2}^2 = m_s^2 m_h^2 - m_{sh}^4 > 0 . \quad (2.15)$$

Alternatively, one can use directly the mass eigenvalues, $m_{s_1}^2, m_{s_2}^2$ and the scalar mixing angle, α_{sh} , as input parameters, imposing the relevant experimental bounds [44] (suitably modified to take the singlet mixing into account).

2.2.1 Stability

We also want that the tree-level potential does not have unbounded-from-below directions. The large-field behaviour of the potential is dominated by the quartic part, which in our parametrization reads:

$$V_4 = \frac{1}{8m_h^2 v^2} [(m_h^2 h^2 + \lambda_m v^2 s^2)^2 + 4\lambda^2 v^4 s^4] . \quad (2.16)$$

For $\lambda_m < 0$, the squared-sum term vanishes along the directions $h = \pm\sqrt{-\lambda_m} v s / m_h$, so that $\lambda^2 > 0$ is required to ensure stability. For $\lambda_m > 0$, on the other hand, the squared-sum term is always positive and the positivity condition on λ^2 can be relaxed but, to maintain stability along the s -direction, one should require $\lambda^2 > -\lambda_m^2/4$ in that case [so that $\lambda_s > 0$ in the parametrization of eq. (2.1)].

The fact that (v, w) is a local minimum does not guarantee that it is the global one: a deeper minimum might exist. We will derive below the necessary and sufficient conditions for this situation to arise. These conditions turn out to be extremely simple in terms of our new parameters.

2.2.2 Local Minima at $\mathbf{h} \neq \mathbf{0}$.

Now we search for further local minima of the potential in order to ensure that (v, w) is the global one or, at least, degenerate with an unbroken minimum (as relevant for the EWPhT). The stationary points of the tree-level potential lie on the curves along which $\partial V / \partial h = 0$,

$$\frac{\partial V}{\partial h} = 0 \Rightarrow \left\{ h = 0 , \quad \text{and} \quad h^2 = D_h^2(s) \equiv \frac{1}{2\lambda_h} (2\mu_h^2 - \mu_m s - \lambda_m s^2) \right\} . \quad (2.17)$$

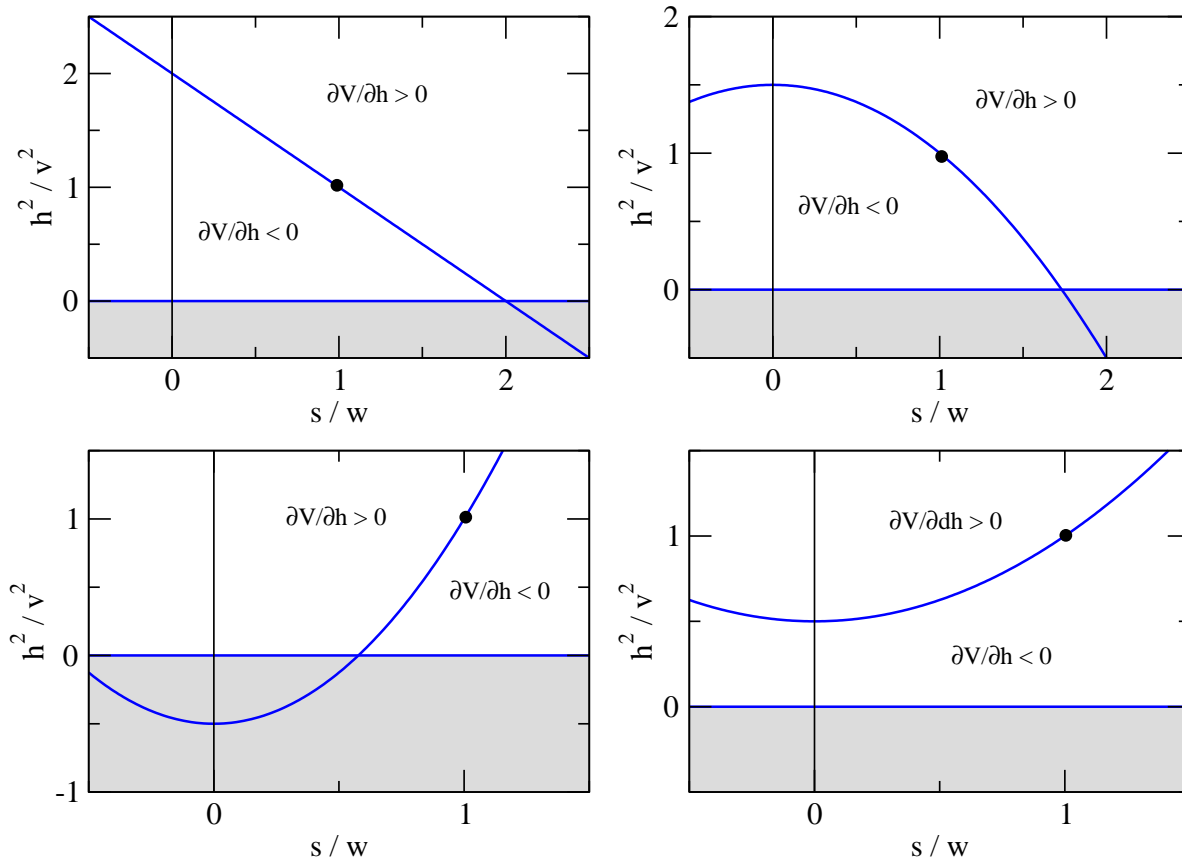


Figure 1: The curve $h^2 = D_h^2(s)$ in the $(h^2/v^2, s/w)$ -plane. The different cases correspond to: $\lambda_m = 0$ (upper left); $\lambda_m > 0$ (upper right); $\lambda_m < 0$ with $|\lambda_m| < m_{sh}^4/(m_h^2 v^2)$ (lower left); $\lambda_m < 0$ with $|\lambda_m| > m_{sh}^4/(m_h^2 v^2)$ (lower right). The unphysical region $h^2 < 0$ is shaded gray. The EW breaking minimum at $h^2 = v^2$ and $s = w$ is marked by a black dot.

In our parametrization, the curve $D_h^2(s)$ reads

$$D_h^2(s) = v^2 - 2v(s-w)\frac{m_{sh}^2}{m_h^2} - \frac{\lambda_m v^2}{m_h^2}(s-w)^2. \quad (2.18)$$

In particular, we have $D_h^2(w) = v^2$ (by construction) and it is interesting that this curve is independent of the parameters m_* , m_s^2 and λ^2 . Its shape, determined by λ_m and m_{sh}^2 , will be relevant later on. Fig. 1 shows the different possibilities for the $D_h^2(s)$ and $h = 0$ lines in the $(h^2/v^2, s/w)$ -plane, with a minimum at $s = w$ as indicated. These lines separate the plane in regions of definite sign of $\partial V/\partial h$.

For $\lambda_m = 0$, the curve $D_h^2(s)$ is a straight line, intersecting the axis $h = 0$ at one single point (Fig. 1, upper left). For the special case in which also $m_{sh}^2 = 0$ one simply has $D_h^2(s) = v^2$, and the corresponding line is parallel to $h = 0$.

In general, with $\lambda_m \neq 0$, $D_h^2(s)$ is a parabola and can have three qualitatively different

forms. If $\lambda_m > 0$, $D_h^2(s)$ curves down and intersects $h = 0$ at two points. If $\lambda_m < 0$, $D_h^2(s)$ curves up. For $|\lambda_m| > m_{sh}^4/(m_h^2 v^2)$, $D_h^2(s)$ does not intersect $h = 0$ while, in the opposite case, it has two intersection points. For either sign of λ_m , the two intersection points with the s -axis are given by

$$s_{\pm} - w = \frac{1}{\lambda_m v} \left[-m_{sh}^2 \pm \sqrt{m_{sh}^4 + \lambda_m v^2 m_h^2} \right]. \quad (2.19)$$

All these different possibilities are illustrated in Fig. 1. We can use the shift freedom to move the axis of the parabola to $s = 0$, which corresponds to enforcing

$$w = \frac{m_{sh}^2}{\lambda_m v}, \quad (2.20)$$

or to setting $\mu_m = 0$ in the original parametrization. This is the choice we generally adopt in our plots.

Next, we consider possible additional stationary points along the curve $h^2 = D_h^2(s)$. The potential along such curve, $V[D_h(s), s]$, is a quartic potential in s that can be minimized in a straightforward manner. More explicitly, the minimization equation $dV[D_h(s), s]/ds = 0$, leads in the general case to a cubic equation of the form

$$a(s - w)^3 + b(s - w)^2 + c(s - w) + d = 0, \quad (2.21)$$

with

$$a = 2\lambda^2 v^2, \quad b = 6m_* v^2, \quad c = \text{Det} \mathcal{M}_s^2, \quad d = 0. \quad (2.22)$$

The nature and number of real solutions this cubic equation has is determined, as usual, by the discriminant

$$\Delta = 18abcd - 4b^3d + b^2c^2 - 4ac^3 - 27a^2d^2. \quad (2.23)$$

For $\Delta < 0$ there is only one real root, corresponding to a single minimum, the electroweak one; for $\Delta > 0$ there are three real roots (the previous minimum and two other stationary points); for $\Delta = 0$ the two additional roots merge in an inflection point. Notice that these additional stationary points are only physically relevant if they appear in the region with $D_h^2(s) > 0$ (the interval $[s_-, s_+]$, with s_{\pm} defined by eq. (2.19), if $\lambda_m > 0$; or the intervals $[-\infty, s_-]$, $[s_+, \infty]$ if $\lambda_m < 0$). With our coordinates,

$$\text{sign}(\Delta) = \text{sign} \left[9m_*^2 v^2 - 2\lambda^2 \text{Det} \mathcal{M}_s^2 \right]. \quad (2.24)$$

Recall that $\text{Det} \mathcal{M}_s^2 = m_s^2 m_h^2 - m_{sh}^4 > 0$ from (2.15). This means that the necessary condition to have an additional stationary point along $D_h^2(s)$ is

$$\lambda^2 < \tilde{\lambda}^2 \equiv \frac{9m_*^2 v^2}{2\text{Det} \mathcal{M}_s^2}, \quad (2.25)$$

where $\tilde{\lambda}^2 > 0$.

In the case $0 < \lambda^2 < \tilde{\lambda}^2$, the two additional stationary points are another minimum and a maximum separating it from the EW breaking one. Their location is also easy to obtain: they appear at $(D_h(w_{\pm}), w_{\pm})$ with

$$w_{\pm} - w \equiv -\frac{3m_*}{2\lambda^2} \pm \frac{1}{2\lambda^2 v} \sqrt{9m_*^2 v^2 - 2\lambda^2 \text{Det}\mathcal{M}_s^2}. \quad (2.26)$$

By evaluating the potential at these points, it is straightforward to obtain the condition for the minimum at (v, w) and the additional one from eq. (2.26) to be degenerate:³

$$\lambda^2 = 8\tilde{\lambda}^2/9. \quad (2.27)$$

For $\lambda^2 < 0$ [which requires $\lambda_m > 0$ from the stability discussion below eq. (2.16)], the two additional stationary points are two maxima, with the EW minimum between them⁴. The EW minimum will still be the deepest (physically relevant) minimum along $D_h^2(s)$ provided $V(v, w) < V(0, s_{\pm})$. If this is not the case, a deeper minimum must exist at $h = 0$. We discuss such situation in the next Subsection.

To summarize, as illustrated by Fig. 2, for a potential with all parameters fixed except λ^2 , the possible stationary points away from $h = 0$ lie along a fixed curve $D_h^2(s)$, independent of λ^2 , with a minimum located at (v, w) by construction. For large enough $\lambda^2 > \tilde{\lambda}^2 > 0$, the minimum at (v, w) is the only stationary point. When $\lambda^2 = \tilde{\lambda}^2$ an inflection point develops, while for smaller λ^2 there are two minima. For $\lambda^2 = 8\tilde{\lambda}^2/9$, the new non-standard minimum is degenerate with the one at (v, w) and for smaller λ^2 our minimum (v, w) is no longer the lowest one. Whether these other minima are physically relevant or not will depend on whether they appear at positive values of $D_h^2(s)$ or not.

2.2.3 Local Minima at $\mathbf{h} = 0$.

To discuss the possible presence of minima in the direction $h = 0$, which might be deeper than the electroweak vacuum, two simple facts are relevant. First, it is useful to note the following relation:

$$V[D_h(s), s] - V[0, s] = -\frac{m_h^2}{8v^2} D_h^4(s) < 0. \quad (2.28)$$

³In this degenerate case, $w_- - w = 2(w_+ - w)$, corresponding to a potential $V[D_h(s), s]$ symmetric under $(s - w_+) \rightarrow -(s - w_+)$ (this is generic for a quartic potential with two degenerate minima).

⁴In this case $V[D_h(s), s]$ is unbounded from below for $s \rightarrow \pm\infty$; however, this is not a problem because this region is not physical when $\lambda_m > 0$, as discussed above eq. (2.24).

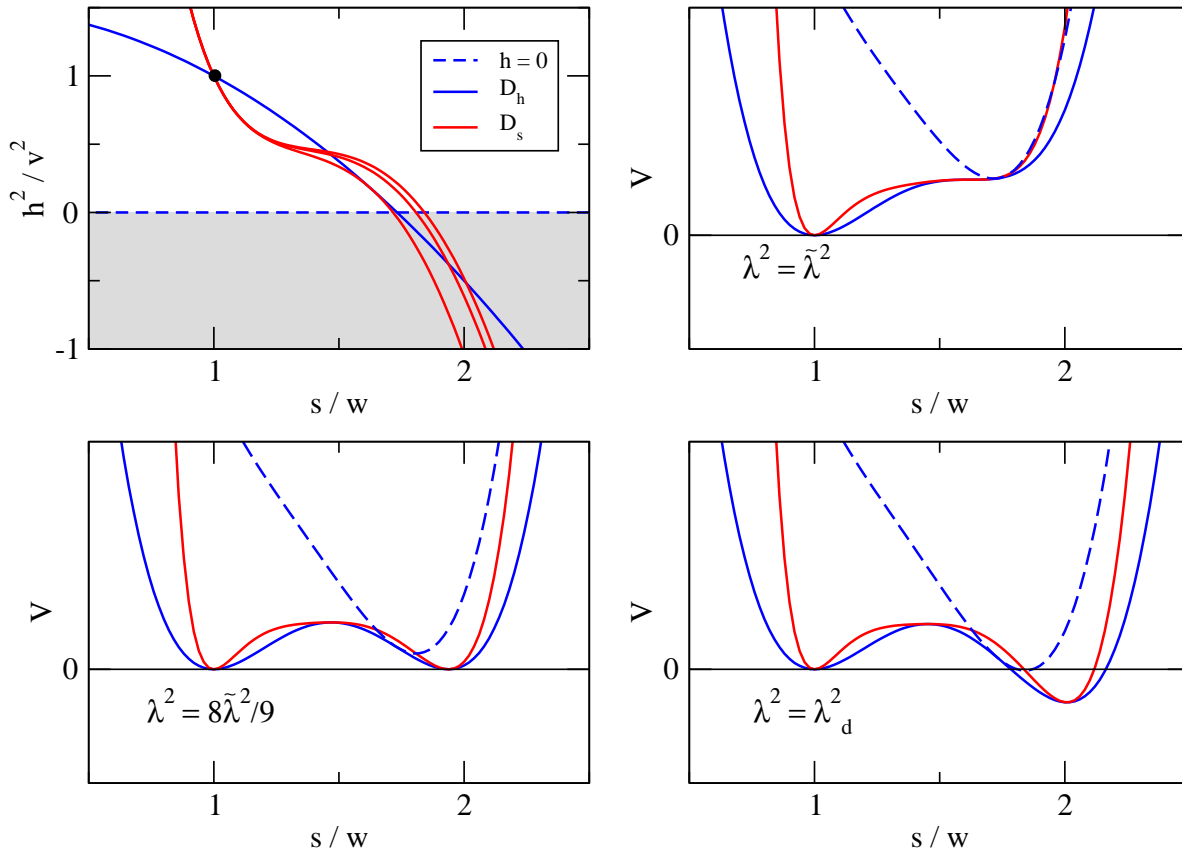


Figure 2: Example for the dependence of the potential on λ^2 . The upper left plot shows $D_h^2(s)$ (solid blue) and $D_s^2(s)$ [along which $\partial V/\partial s = 0$, see eq. (2.35)] (solid red) for several values of λ^2 : $\tilde{\lambda}^2$, $8\tilde{\lambda}^2/9$ and λ_d^2 . The intersections of these two curves correspond to the stationary points of the potential. The remaining plots show the potential along $D_h^2(s)$, $D_s^2(s)$ (same color coding) and $h = 0$ (dashed) at the indicated values of λ^2 .

A glance at Fig. 1 explains this fact as a result of the sign of $\partial V/\partial h$ in the region between the lines $h = 0$ and $h^2 = D_h^2(s)$. Second,

$$\left. \frac{\partial^2 V[h, s]}{(\partial h)^2} \right|_{h=0} = -\frac{m_h^2}{2v^2} D_h^2(s). \quad (2.29)$$

This implies that minima along $h = 0$ can only appear in regions with $D_h^2(s) < 0$.⁵ Moreover, in order to locate such minima, it is enough to minimize $V[0, s]$: if a minimum found in this way appears at $D_h^2(s) < 0$, then (2.29) ensures that it is also a minimum along the h -direction. We also conclude that, for fixed s the potential can have only one minimum: at $h = 0$ for $D_h^2(s) < 0$ or at $h \neq 0$ for $D_h^2(s) > 0$.

More can be said about these minima at $h = 0$ by considering the following general

⁵An alternative way to see this is to note that $\partial^2 V/(\partial h)^2 = 0$ along the line $h^2 = D_h^2(s)/3$, which divides the (h^2, s) -plane in two regions with opposite signs of $\partial^2 V/(\partial h)^2$.

statement about the tree-level potential: *If there are two local minima with $h^2 > 0$ then there is no local minimum with $h = 0$.* To prove this, assume there are two local minima with $h^2 > 0$ and one with $h = 0$, chosen to be the absolute minimum along $h = 0$ and to lie at $s = 0$. Consider a curve of the form

$$h^2 = D^2(s) \equiv \alpha s + \beta s^2 = \beta s(s - s_1) , \quad (2.30)$$

that passes through all three minima (two minima with equal s are not possible and so, this curve always exists). The potential along this curve, $V_D(s) \equiv V[D(s), s]$, is a quartic polynomial and, therefore, can have at most three stationary points. Two of them are the two minima with $h^2 > 0$ while the minimum at $h = 0$ is in general not a stationary point of $V_D(s)$. The reason is that $dV[D(s), s]/ds = [dV/d(h^2)]dD^2(s)/ds + dV/ds$, but $dV/dh = 0$ does not in general imply $dV/d(h^2) = 0$ because $h = 0$ leads to $dV/dh = 0$ even if $dV/d(h^2) \neq 0$.⁶ Furthermore, minima must be separated by maxima and in most geometrical arrangements of the locations of the three minima this will require more stationary points than the allowed maximum of three. The only non-trivial case occurs if the minimum at $h = 0$ is between the other two (ordered by their s -coordinates) and $s_1 \neq 0$, but in that case it is straightforward to see that $V_D(s_1) < V_D(0)$, contradicting our assumption that $s = 0$ is the absolute minimum along $h = 0$, and this concludes the proof.⁷

On the other hand, *if there is only one local minimum with $h^2 > 0$ there can be up to two local minima with $h = 0$.* The case with two minima at $h = 0$ requires that the potential $V_D(s)$ has one minimum (the one corresponding to $h \neq 0$) and is negative for $s \rightarrow \pm\infty$. In addition, the two minima at $h = 0$ lie at both sides of the EW minimum. (An explicit example will be given in the \mathbf{Z}_2 symmetric case below).

Having these facts in mind, we can compare minima at $h = 0$ with our minimum (v, w) and discuss what are the conditions on the parameters of the potential for (v, w) to be the global minimum. We will illustrate this with an example in Fig. 2, which plots the potential along $h^2 = D_h^2(s)$ and $h = 0$ for different values of λ^2 . Consider first the case in which (v, w) is the deepest minimum of $V[D_h(s), s]$ (i.e. we have $\lambda^2 > 8\tilde{\lambda}^2/9$), then (2.28) immediately implies it should also be the global minimum of $V[h, s]$. Such case is shown in Fig. 2, upper right plot. Cases with $\lambda^2 < 8\tilde{\lambda}^2/9$, for which a deeper minimum along $D_h^2(s)$ appears (or, if $\lambda^2 < 0$, when $V[D_h(s), s]$ is unbounded from below), might still have (v, w) as the global minimum (this happens if the new minimum is in the unphysical region, $D_h^2(s) < 0$), as in Fig. 2, lower left plot. In such cases one needs to check the minima along $h = 0$, which might

⁶A relevant exception to this is $h^2 = D_h^2(s)$ as then we always have $dV/d(h^2) = 0$ by construction.

⁷Obviously, this "theorem" applies to the tree-level potential only and can be violated through loop corrections. It is nevertheless useful in order to identify large barriers created by tree-level effects.

be deeper than the EW one without violating (2.28). As λ^2 gets more and more negative, minima along $h = 0$ might become the global minimum. In general, when all parameters except λ^2 are fixed, the potential along $h = 0$ decreases with decreasing λ^2 [see the explicit potential in eq. (2.14)]. Hence, there is a definite value λ_d^2 for λ^2 that separates the region in parameter space in which the EW minimum is the deepest one from the one where it is not. It is clear that $-\lambda_m^2/4 \leq \lambda_d^2 \leq 8\tilde{\lambda}^2/9$. The exact value of λ_d^2 will be determined below by requiring degeneracy between the EW minimum and the second minimum [see eq. (2.43)], an example of which is shown in the lower right plot of Fig. 2. Studying such degenerate cases will be very relevant for the discussion of strong phase transitions in the next Section, so we turn to this issue next.

2.3 Coexisting and Degenerate Minima.

The most interesting cases for the phase transition study are potentials with two degenerate minima: the EW-breaking one, at (v, w) , and the symmetric one at $(0, w_0)$. While we could use the shift of eq. (2.2) to specify the value of the singlet field VEV in the unbroken phase, w_0 ($w_0 = 0$ is often used in the literature), here we will keep again the shift-invariance explicit since, in our parametrization, such choice would simplify intermediate expressions only marginally.

We will next show that, out of the eight initial parameters, only three have an impact on the *shape* features of the potentials with two degenerate minima. Two parameters can be removed thanks to the shift-symmetry and the requirement of degeneracy of the minima. Two more parameters can be removed by rescaling the potential in the s and h directions. Finally the overall scale of the potential has no qualitative meaning in this discussion, leaving us with three parameters. In the following we present a parameter choice, a refinement with respect to eqs. (2.7)-(2.13), which is especially handy in describing the qualitative features of a potential with degenerate minima.

To discuss the minima, let us consider the curves $\partial V/\partial h = 0$ and $\partial V/\partial s = 0$ more systematically. The curves $h = 0$ and $D_h^2(s)$, at which $\partial V/\partial h = 0$, were already introduced in eqs. (2.17). We begin with $\lambda_m \neq 0$, in which case we can rewrite the curve $D_h^2(s)$ as:

$$D_h^2(s) = \bar{h}^2 - \frac{\lambda_m v^2}{m_h^2} (s - w_p)^2, \quad (2.31)$$

where, using both the notation of eqs. (2.7)-(2.13) and the original notation,

$$\bar{h}^2 \equiv v^2 + \frac{m_{sh}^4}{\lambda_m m_h^2} = \frac{1}{\lambda_h} \left(\mu_h^2 + \frac{\mu_m^2}{8\lambda_m} \right), \quad (2.32)$$

$$w_p \equiv w - \frac{m_{sh}^2}{\lambda_m v} = -\frac{\mu_m}{2\lambda_m}. \quad (2.33)$$

In the plots, we will generally choose our singlet coordinates to have $w_p = 0$ (setting $\mu_m = 0$), so that the parabola $D_h^2(s)$ has its axis at $s = 0$. As discussed in Section 2, the minimum at $h = 0$ can only be located in the regions with $D_h^2(w_0) < 0$.

The potential is a quartic in s and hence has at most three extrema with respect to s for fixed h (out of which at most two are minima). For general values of h ,

$$\frac{\partial V}{\partial s} = \frac{1}{4} h^2 (\mu_m + 2\lambda_m s) + (\mu_1^3 + \mu_s^2 s + \mu_3 s^2 + \lambda_s s^3), \quad (2.34)$$

and the curve $\partial V/\partial s = 0$ in the (h^2, s) -plane as a function of s is given by

$$h^2 = D_s^2(s) \equiv -4 \frac{\mu_1^3 + \mu_s^2 s + \mu_3 s^2 + \lambda_s s^3}{\mu_m + 2\lambda_m s}, \quad (2.35)$$

or, in our parametrization:

$$D_s^2(s) = v^2 - \frac{(s-w)}{\lambda_m m_h^2 (s-w_p)} \left[2m_h^2 m_s^2 + 3v(\lambda_m m_{sh}^2 + 4m_* v)(s-w) + (4\lambda^2 + \lambda_m^2)(s-w)^2 \right]. \quad (2.36)$$

This function is single-valued for fixed s and has a pole at $s = w_p$. When this pole is canceled by a zero of the numerator, the line $s = w_p$ is also a solution of $\partial V/\partial s = 0$ (this is e.g. the case for a potential with a \mathbf{Z}_2 symmetry $s \rightarrow -s$) and enters the discussion. The asymptotic behavior of $D_s^2(s)$ at large s is $D_s^2(s) \rightarrow -2\lambda_s s^2/\lambda_m$ and hence is qualitatively different depending on the sign of λ_m . In the following, we distinguish four different cases given by⁸

$$(a) \quad \lambda_m < 0, \quad (w_0 - w_p)(w - w_p) > 0, \quad (2.37)$$

$$(b) \quad \lambda_m < 0, \quad (w_0 - w_p)(w - w_p) < 0, \quad (2.38)$$

$$(c) \quad \lambda_m > 0, \quad (w_0 - w_p)(w - w_p) < 0, \quad (2.39)$$

$$(d) \quad \lambda_m > 0, \quad (w_0 - w_p)(w - w_p) > 0. \quad (2.40)$$

The sign of λ_m determines whether the parabola $D_h^2(s)$ curves up or down. The sign of $(w_0 - w_p)(w - w_p)$ determines if the two minima lie at the same side or different sides of the

⁸The case $w_0 = w_p$ is only possible for $\lambda_m < 0$ and smoothly connects cases (a) and (b). This case will be very relevant in the particular scenario of Section 4. The case $w = w_p$, on the other hand, is only possible for $\lambda_m > 0$ and smoothly connects cases (c) and (d).

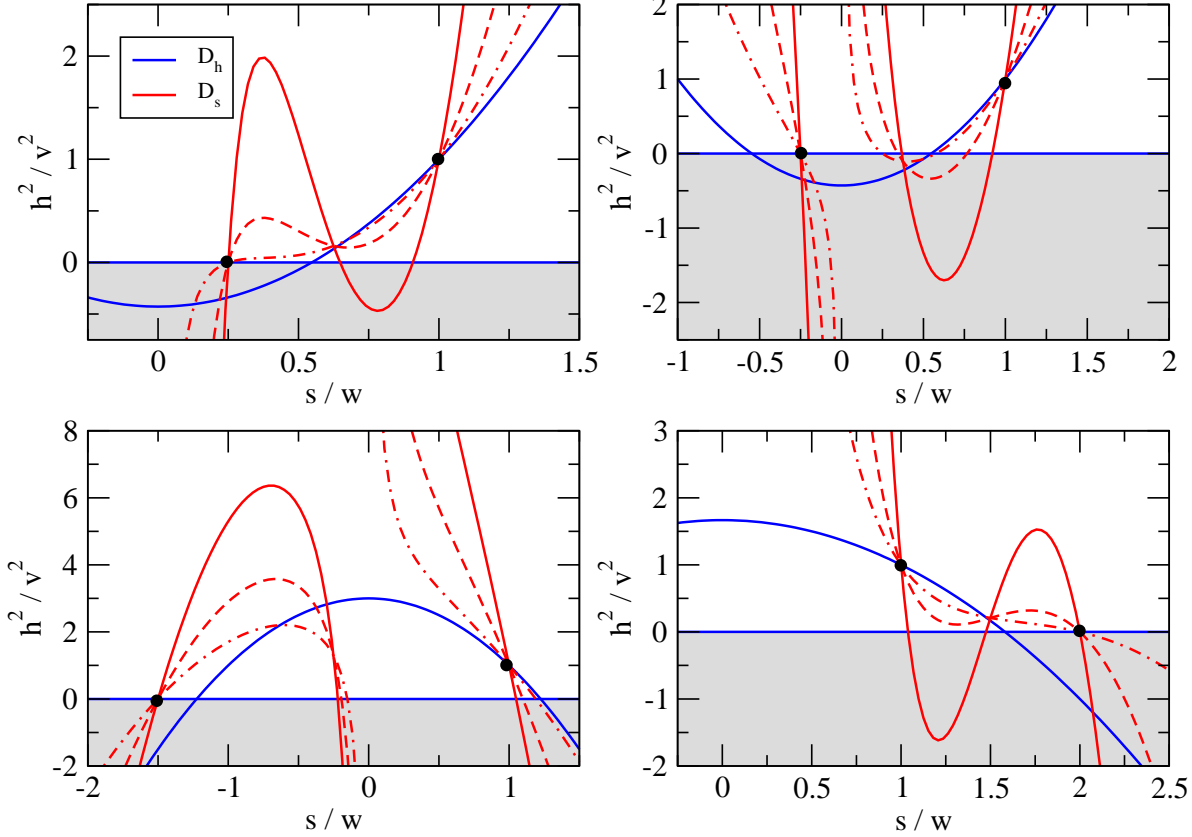


Figure 3: Curves $D_h^2(s)$ (solid blue) and several $D_s^2(s)$ (red solid, dashed and dash-dotted) with different values of m_s^2 , intersecting to give two potential minima (indicated by black dots) in the 4 different cases listed in eqs. (2.37)-(2.40).

pole at $s = w_p$. Examples for the curves $D_s^2(s)$ and $D_h^2(s)$ in these four cases are depicted in Fig. 3. Is it obvious that, once we have two degenerate minima in our potential, there is a barrier separating them. The two minima and the saddle point in between appear at the intersections between the $D_h^2(s)$ and $D_s^2(s)$ curves, which must be of sufficiently high degree to allow for such structure.⁹ The different cases listed above will in general lead to different shapes of the potential barriers, which have an impact on the profile of the critical bubbles for the EWPhT.

It is convenient to introduce a different parametrization for this degenerate case, that can be easily connected to the qualitative features of the curves $D_h^2(s)$ and $D_s^2(s)$. Remember that the solutions of $\partial V/\partial s = 0$ at the axis $h = 0$ lead to a cubic equation and up to two local minima that are cumbersome to determine analytically. To avoid this problem, it is

⁹Some analysis in the literature solve the equation $\partial V/\partial s = 0$ for $s(h)$ and then look for a barrier in the one-dimensional potential $V[h(s), s]$. While this is justified in some cases, Fig. 3 illustrates some of the possible dangers of this procedure: $h(s)$ might not be single-valued; $V[h(s), s]$ can venture into the unphysical region; and sometimes there is no continuous path connecting both minima and having $\partial V/\partial s = 0$.

helpful to treat the position of the minimum w_0 as a free parameter and trade it for the parameter m_* . Imposing the condition that both minima are degenerate, the parameter λ^2 can be fixed. Finally, one can also trade the parameter m_{sh}^2 for w_p , the point that marks the axis of symmetry of the curve $D_h^2(s)$. We end up with the following parameters

$$\{w, w_p, w_0, v, m_h^2, m_s^2, \lambda_m\} , \quad (2.41)$$

related to the ones in eq. (2.6) by

$$m_* = \frac{\Delta w}{4} \left\{ -\lambda_m \left[\frac{m_h^2}{\Delta w^2} + \frac{m_{sh}^2}{v\Delta w} \right] + \frac{m_h^2}{\Delta w^2} \left[\frac{m_h^2}{\Delta w^2} + 2\frac{m_s^2}{v^2} + 3\frac{m_{sh}^2}{v\Delta w} \right] \right\} , \quad (2.42)$$

$$\lambda^2 = \lambda_d^2 \equiv -\frac{1}{4} \left[\lambda_m + \frac{m_h^2}{\Delta w^2} \right]^2 + \frac{m_h^2}{\Delta w^2} \left[\frac{m_h^2}{\Delta w^2} + \frac{m_s^2}{v^2} + 2\frac{m_{sh}^2}{v\Delta w} \right] , \quad (2.43)$$

$$m_{sh}^2 = \lambda_m v (w - w_p) , \quad (2.44)$$

where¹⁰ $\Delta w \equiv w - w_0$ and, as promised, we give the expression for λ_d^2 , the value of λ^2 required for degeneracy of the minima (and already discussed at the end of SubSection 2.2.3). Some of the particular combinations of masses that appear above have a direct physical interpretation. For instance, we have

$$\frac{m_h^2}{\Delta w^2} + \frac{m_s^2}{v^2} + 2\frac{m_{sh}^2}{v\Delta w} = \left(\frac{1}{v^2} + \frac{1}{\Delta w^2} \right) m_\varphi^2 , \quad (2.45)$$

where m_φ^2 is the squared mass at the broken minimum along the direction $\varphi \equiv s \cos \theta + h \sin \theta$ (that joins both minima), where the angle θ satisfies $\tan \theta = v/\Delta w$.

Finally, we can now obtain the condition necessary to ensure that w_0 is the deepest minimum along $h = 0$, which simply reads:

$$\text{Det} \mathcal{M}_s^2 > \frac{v^2}{\Delta w^2} (m_h^2|_0) m_h^2 , \quad (2.46)$$

where $m_h^2|_0$ is the squared-mass $\partial^2 V / (\partial h)^2$ at the symmetric minimum $(0, w_0)$, which is given by

$$m_h^2|_0 = \frac{\Delta w^2}{2} \left[\lambda_m - \frac{m_h^2}{\Delta w^2} - 2\frac{m_{sh}^2}{v\Delta w} \right] > 0 . \quad (2.47)$$

It is interesting that these conditions also ensure that the potential is bounded from below: that is, if (2.46) and (2.47) are satisfied then λ^2 fulfills the stability constraints discussed in SubSection 2.2.1.

The fact that the quantities in the discussion above depend always on the ratios $R_h \equiv m_h^2/\Delta w^2$, $R_s \equiv m_s^2/v^2$ and $R_{sh} \equiv m_{sh}^2/(v\Delta w)$ (plus λ_m) is a consequence of the fact that, as

¹⁰ Δw cannot be zero in the presence of a barrier, and therefore, at the EWPhT there is a jump both in $\langle h \rangle$ and $\langle s \rangle$. This can be important for some EW baryogenesis mechanisms.

we mentioned earlier, the conditions for degeneracy are independent of possible rescalings of the fields h and s . If such field rescaling is followed by a global rescaling of the potential so as to leave λ_m unchanged, the above ratios are also invariant under such combination of rescalings. Multiplying these 4 parameters by a common factor changes the potential by the same overall factor and so, the shape of the potential with two degenerate minima is determined by just 3 shape parameters: the three independent ratios $\{\lambda_m/R_h, R_{sh}/R_h, R_s/R_h\}$.

The potential with such degenerate vacua takes the form

$$V = \frac{1}{8}v^2m_h^2 \left\{ (h_r^2 - 1)^2 + (s_r - 1)^3(1 + 3s_r) + 2\frac{\lambda_m}{R_h}(s_r - 1)^2(h_r^2 - s_r^2) + 4\frac{R_s}{R_h}s_r^2(s_r - 1)^2 + 4\frac{R_{sh}}{R_h}(s_r - 1)[h_r^2 + s_r^2(2s_r - 3)] \right\}, \quad (2.48)$$

where we have used

$$h_r \equiv \frac{h}{v}, \quad s_r \equiv \frac{s - w_0}{\Delta w}, \quad (2.49)$$

with the EW minimum at $h_r = 1, s_r = 1$ and the symmetric one at $h_r = s_r = 0$.

The previous discussion assumes $\lambda_m \neq 0$, but one can also get degenerate minima for $\lambda_m = 0$. In that case, the curve $D_h^2(s)$ becomes a straight line and reads

$$h^2 = D_h^2(s) = v^2 - 2v(s - w)\frac{m_{sh}^2}{m_h^2}, \quad (2.50)$$

intersecting the axis $h = 0$ at

$$w_x = w + \frac{m_h^2 v}{2m_{sh}^2}. \quad (2.51)$$

We can again impose degeneracy of the two vacua, and write m_* in terms of w_0 , as we did for $\lambda_m \neq 0$, arriving at the same eqs. (2.42) and (2.43); on the other hand, m_{sh}^2 is now fixed by (2.51):

$$m_{sh}^2 = \frac{m_h^2 v}{2(w_x - w)}. \quad (2.52)$$

The parameters to describe the potential with degenerate minima in the case $\lambda_m = 0$ are then

$$\{w, w_x, w_0, v, m_h^2, m_s^2\}. \quad (2.53)$$

2.3.1 Flat Directions

An intriguing situation occurs in the particular limiting case in which $D_{h,s}^2(s)$ fall on top of each other; then these curves correspond to a flat direction of the potential. In terms of the

original potential parameters, $D_h^2(s) \equiv D_s^2(s)$ requires

$$\mu_h^2 \mu_m + 4\lambda_h \mu_1^3 = 0 , \quad (2.54)$$

$$4\lambda_m \mu_h^2 - \mu_m^2 + 8\lambda_h \mu_s^2 = 0 , \quad (2.55)$$

$$8\lambda_h \mu_3 - 3\lambda_m \mu_m = 0 , \quad (2.56)$$

$$4\lambda_h \lambda_s - \lambda_m^2 = 0 , \quad (2.57)$$

which, in terms of our parameters, simply read¹¹

$$\lambda^2 = 0 , \quad m_* = 0 , \quad \text{Det} \mathcal{M}_s^2 = 0 . \quad (2.58)$$

While these conditions would be unacceptable at $T = 0$, we will see in later Sections that, if such flat direction develops at the critical temperature for the electroweak phase transition, the strength of this transition can be significantly larger: the small effect from thermally induced cubic terms in the finite-temperature potential is enhanced along such flat directions.

Imposing the conditions derived above, the potential takes the simple form

$$V = \frac{1}{8m_h^2 v^2} [m_h^2 (h^2 - v^2) + \lambda_m v^2 (s - w)^2 \pm 2m_h m_s v (s - w)]^2 , \quad (2.59)$$

where the \pm sign corresponds to the possible sign of m_{sh}^2 . The flat direction will in general be parabolic in the (h^2, s) -plane, becoming a straight line for $\lambda_m = 0$. We will examine this scenario in more detail in the following Sections.

3 Strong Electroweak Phase Transitions

The present model can develop very strong phase transitions if the barrier separating the broken and symmetric vacua is produced by tree-level effects (as discussed in the previous Section) and not by the cubic term resulting from one-loop thermal contributions of bosons (which is the most studied mechanism to achieve a first-order phase transition). Indeed, the latter are always proportional to the temperature and lead to a critical order parameter $v_c \propto T_c$. In this case the strength of the EWPhT, characterized by v_c/T_c , is independent of the temperature and typically proportional to small couplings. For a tree-level barrier, on the other hand, v_c is proportional to other dimensionful parameters of the potential and almost T-independent¹². In this case v_c/T_c can be large for small critical temperatures.

¹¹Here there are only three conditions, since the shift symmetry has not been used to fix one of the parameters in the original parametrization. In (2.58), on the other hand, this degree of freedom disappears since the parameters are shift-independent.

¹²Incidentally, due to this property the strength of such transitions will be insensitive to the gauge-fixing subtleties discussed in [45].

3.1 Evolution of Parameters at Finite T

When the barrier is produced at tree-level, it is enough to include in the one-loop thermal potential the leading terms in the high-temperature expansion that lift the minimum in the broken phase. In our model, these terms are

$$V_{1-loop}^{T \neq 0} = \left(\frac{1}{2} c_h h^2 + \frac{1}{2} c_s s^2 + m_3 s \right) T^2, \quad (3.1)$$

where

$$\begin{aligned} c_h &= \frac{1}{48} \left[9g^2 + 3g'^2 + 2(6h_t^2 + 12\lambda_h + \lambda_m) \right], \\ c_s &= \frac{1}{12} (2\lambda_m + 3\lambda_s), \\ m_3 &= \frac{1}{12} (\mu_3 + \mu_m). \end{aligned} \quad (3.2)$$

Here g and g' are the $SU(2)_L$ and $U(1)_Y$ gauge couplings and h_t is the top Yukawa coupling. Additional particles coupled to the Higgs or the singlet will in general contribute to these quantities. At very high temperature the potential is dominated by this contribution, which drives $\langle h \rangle \rightarrow 0$, restoring the EW symmetry [46]. On the other hand, the singlet develops a thermal tadpole so that $\langle s \rangle \rightarrow s_\infty = -m_3/c_s$ at high T .¹³ In the general case, without an $s \rightarrow -s$ symmetry, there is no reason to expect $s \rightarrow 0$. This could be arranged by using the coordinate frame $\mu_3 = -\mu_m$ (provided $c_s > 0$) but there is no sense in which a symmetry associated with the singlet is being restored, simply because there is no symmetry.¹⁴

The key point in our approach is that the terms in (3.1) can be absorbed in the definition of T -dependent parameters

$$\begin{aligned} -\mu_h^2(T) &\equiv -\mu_h^2 + c_h(T^2 - T_c^2), \\ \mu_s^2(T) &\equiv \mu_s^2 + c_s(T^2 - T_c^2), \\ \mu_1^3(T) &\equiv \mu_1^3 + m_3(T^2 - T_c^2), \end{aligned} \quad (3.3)$$

where we use a notation in which, when no temperature is indicated for some T -dependent quantity, it is implicitly assumed that its value at T_c is meant, *e.g.* $m_s^2 \equiv m_s^2(T_c)$. We can then apply the general results on the structure of the potential derived in Section 2. The minima are still determined by the curves $D_h^2(s)$ and $D_s^2(s)$, which are now T -dependent and induce a T -dependence in the location of the minima. We have

$$\frac{dD_h^2(s)}{dT^2} = -\frac{c_h}{\lambda_h}, \quad \frac{dD_s^2(s)}{dT^2} = -\frac{4(m_3 + c_s s)}{\mu_m + 2\lambda_m s}. \quad (3.4)$$

¹³Under a singlet shift, $m_3 \rightarrow m_3 + c_s \sigma$, so that s_∞ transforms as it should.

¹⁴In the case with a \mathbf{Z}_2 -symmetric potential thermal corrections do not break the symmetry and $s \rightarrow 0$ at high T , restoring the symmetry in the vacuum.

The curve $D_h^2(s)$ approaches the axis $h = 0$ as T increases (keeping fixed its symmetry axis and without changing its shape); this guarantees that $v \rightarrow 0$ at high T . The evolution of $D_s^2(s)$ is more complicated in general. We can simplify somewhat the analysis by choosing $\mu_m = 0$ through the shift-symmetry, and then we have

$$\frac{dD_s^2(s)}{dT^2} = -\frac{2}{\lambda_m} \left(c_s - \frac{m_3}{s} \right), \quad (\mu_m = 0). \quad (3.5)$$

Now, for the cosmological history from T_c to $T = 0$ to be acceptable, the EW minimum must be the global one at $T = 0$: $V_b(0) < V_s(0)$. This requirement will put a constraint on the parameters of the potential. The evolution of the difference $\Delta V_{bs}(T) \equiv V_b(T) - V_s(T)$ with T can be determined as follows:

$$\frac{d\Delta V_{bs}(T)}{dT^2} = \sum_i \left[\left. \frac{\partial V}{\partial \mu_i^2} \right|_b - \left. \frac{\partial V}{\partial \mu_i^2} \right|_s \right] \frac{d\mu_i^2}{dT^2} + \sum_\alpha \left[\left. \frac{\partial V}{\partial \phi_\alpha} \right|_b \frac{d\langle \phi_\alpha \rangle_b}{dT^2} - \left. \frac{\partial V}{\partial \phi_\alpha} \right|_s \frac{d\langle \phi_\alpha \rangle_s}{dT^2} \right], \quad (3.6)$$

where we symbolically write $\mu_i^2 \equiv \{\mu_h^2, \mu_s^2, \mu_1^3\}$, $\phi_\alpha \equiv \{h, s\}$. Noting that $\partial V / \partial \phi_\alpha = 0$ at both minima and using the T dependence of the μ_i^2 parameters from eq. (3.3), we obtain

$$\frac{d\Delta V_{bs}(T)}{dT^2} = \frac{1}{2} \{ c_h v^2(T) + \Delta w(T) (c_s [w(T) + w_0(T)] + 2m_3) \}, \quad (3.7)$$

(which is a shift-invariant expression, see footnote 13). A necessary condition for the EWPhT to take place is that this derivative is positive at T_c so that the broken minimum is the deepest one at least for $T \lesssim T_c$,

$$\left. \frac{d\Delta V_{bs}(T)}{dT^2} \right|_{T_c} = \frac{1}{2} \{ c_h v^2 + \Delta w (c_s [w + w_0] + 2m_3) \} > 0. \quad (3.8)$$

Note, however, that this is a necessary but not sufficient condition to guarantee that (v, w) is the global minimum at $T = 0$: this must be checked separately, as summarized in Table 1, and as will be shown in particular examples in later Sections.

3.2 Strategy to Identify Strong EWPhTs

What are the regions of parameter-space that lead to a tree-level barrier? In terms of the original parameters of the potential in eq. (2.1), the answer to this question generally involves a complicated superposition of non-linear conditions, with hidden physical meaning and hard to use for phenomenological applications. This task is greatly simplified by the parametrization introduced in Section 2, which allows an easy identification of a potential with stable minima. Moreover, when minima exists they must necessarily be separated by

	Parameters	Conditions
$T = T_c$ Degenerate V , (2.48)	$\{w, w_p, w_0,$ $v, m_h^2, m_s^2, \lambda_m\}$	Stability in w_0 and w , (2.46)-(2.47) : $\text{Det}\mathcal{M}_s^2 > (v^2/\Delta w^2)(m_h^2 _0)m_h^2$ $m_h^2 _0, m_h^2, m_s^2 > 0$
Matching	$\lambda^2 = \lambda_d^2$ $m_* = m_*(w_0)$ $m_{sh}^2 = m_{sh}^2(w_p)$	Broken min. deepest, (3.8) : $d\Delta V_{bs}(T)/dT^2 _{T_c} > 0$
$T \leq T_c$ General V , (2.14)	$\{v, w, m_h^2, m_s^2,$ $m_{sh}^2, \lambda_m, \lambda^2, m_*\}$	V bounded below, (2.16) : $\lambda^2 > 0$ ($\lambda_m \leq 0$) $\lambda^2 > -\lambda_m^2/4$ ($\lambda_m > 0$) Vacuum stability, (2.15) : $\text{Det}\mathcal{M}_s^2 > 0$ $m_h^2, m_s^2 > 0$ Global min., (2.27) : $\lambda^2 \geq 8\tilde{\lambda}^2/9$

Table 1: Summary on the strategy and parameter conditions to identify potentials with large tree-level barriers.

a barrier. Indeed, any potential of the general form (2.14), has a stable global minimum at (v, w) for any values of the parameters $\{v, w, m_h^2, m_s^2, m_{sh}^2, \lambda_m, \lambda^2, m_*\}$ if the simple conditions discussed below eqs. (2.15),(2.16) and (2.27) are fulfilled. Similarly, a potential of the degenerate form (2.48), with parameters $\{w, w_p, w_0, v, m_h^2, m_s^2, \lambda_m\}$ satisfying the conditions of eqs. (2.46)-(2.47), has a barrier between two degenerate minima at (v, w) and $(0, w_0)$. Both cases are summarized in Table 1.

Hence, the strategy to find a model with a strong phase transition is the following, as illustrated in Table 1. First, choose a value for the parameters $\{w, w_p, w_0, v, m_h^2, m_s^2, \lambda_m\}$, subject to the simple conditions summarized in the upper part of Table 1. Any such choice determines a potential of the form (2.48) with two degenerate minima with broken and unbroken EW symmetry and a barrier separating them: this will be the thermal potential at some critical temperature T_c , which at this point we are free to choose. Once we select T_c , we can match this potential to a general potential (2.14), making sure to satisfy the conditions in the middle part of Table 1, which ensure that the broken minimum gets deeper than the symmetric minimum for decreasing $T \lesssim T_c$. Finally, using the formulae outlined in the previous Subsection, we can evolve all the parameters with T to obtain their values at $T = 0$: these are the relevant parameters that enter physically meaningful quantities like the

scalar masses, mixings, etc. As T is lowered, it is crucial that our (broken) vacuum remains the global stable minimum of the potential: this is guaranteed by the conditions in the lower part of Table 1. In fact, the stability conditions on λ^2 are guaranteed to be satisfied once the T_c parameters satisfy the conditions in the upper part of Table 1. Eventually, h and s should be suitably rescaled to ensure that the zero temperature vev is $v = v_{EW}$. In this way, different values of T_c will generate a family of models with different values of the potential parameters, but all with the same potential shape at T_c .

With the zero temperature potential at hand, a full-fledged one-loop analysis can be performed to confirm the first-order nature of the phase transition and to calculate the real critical temperature at which the broken and symmetric vacua are degenerate. This temperature will in general differ from the T_c parameter we have used, which corresponds in the mean-field approximation to the real critical one. We call $T_{c,MF}$ the latter and $T_{c,1L}$ the former. We will show this strategy at work in some examples in later Sections. The details of the calculation of the one-loop scalar potential at finite T , which are standard, are relegated to Appendix A.

Notice that our estimate of v_c/T_c is conservative since the true critical temperature at which the transition starts (the nucleation temperature) is smaller than our T_c . For a complete analysis, one should also recalculate how the sphaleron energy is affected by the Higgs barrier and how this impacts the critical ratio v_c/T_c required for a successful preservation of the baryon asymmetry. However, it is generically the case that the sphaleron energy is dominated by gauge degrees of freedom with Higgs effects amounting to a few percent change (see *e.g.* [47]).

Before moving to the examples, let us finally mention the case in which the potential has two degenerate minima but both with $h > 0$. Does this correspond to some situation of physical interest? We know that, also in such cases, the EW symmetry will be restored at some higher temperature and a local minimum at $h = 0$ will arise, at which point there can be only one broken minimum (as we showed in the previous Section). Hence, in this case either the two broken minima merge together or one of them moves to $h = 0$ before the critical temperature is reached. Both options correspond to peculiar phase transition histories and merit study, which we leave for a future analysis.

4 Special Cases: \mathbf{Z}_2 -symmetric Potential

In a general study like this one, concentrating on the potential (2.1) which involves many parameters, it is crucial to identify whether or not some regions of parameter space are more natural than others. This point is especially relevant in the presence of symmetries, which select a region of parameter space with vanishing volume (and hence unlikely from the point of view of a general analysis) and preserve it under RG-evolution and at finite temperature. For the SM plus a singlet, the only symmetry (both of the kinetic terms and of the potential at renormalizable level) that is interesting from the point of view of the EWPhT is the \mathbf{Z}_2 symmetry $s \rightarrow -s$. One particular case of interest that falls in this category is the so-called Singlet Majoron Model [9]. The EWPhT in this model has been studied in [14].¹⁵

Making the \mathbf{Z}_2 symmetry manifest (although the general analysis of Section 2 can be carried out without problem), the potential is of the form given in eq. (2.1) with

$$\mu_1 = 0, \quad \mu_m = 0, \quad \mu_3 = 0. \quad (4.1)$$

In terms of our parameters (2.6), these constraints translate into two separate branches, depending on whether the \mathbf{Z}_2 -symmetry is broken spontaneously or not. The \mathbf{Z}_2 -symmetric case has

$$w = 0, \quad m_* = 0, \quad m_{sh}^2 = 0, \quad (4.2)$$

and the \mathbf{Z}_2 -broken case has $w \neq 0$ and

$$m_s^2 = 2\lambda_s w^2 = (4\lambda^2 + \lambda_m^2) \frac{v^2 w^2}{m_h^2}, \quad m_{sh}^2 = \lambda_m v w, \quad m_* = \lambda^2 w, \quad (4.3)$$

which allows to extract the usual parameters w , m_* and m_{sh}^2 in terms of the others:

$$w = \frac{m_h m_s}{v \sqrt{4\lambda^2 + \lambda_m^2}}, \quad m_* = \lambda^2 \frac{m_h m_s}{v \sqrt{4\lambda^2 + \lambda_m^2}}, \quad m_{sh}^2 = \lambda_m \frac{m_h m_s}{\sqrt{4\lambda^2 + \lambda_m^2}}. \quad (4.4)$$

This model can then be described by the 5 parameters $\{v, m_h^2, m_s^2, \lambda_m, \lambda^2\}$ in both branches but, to avoid confusion, the first part of this Section will be clearer in the standard notation of eq. (2.1).

At high temperature we expect the minimum to lie at the symmetric point $h = 0$, $s = 0$ but it might happen that $s \neq 0$ prior to the EWPhT. The stationary points of the potential will be determined by the intersections of the curves $\partial V/\partial h = 0$ and $\partial V/\partial s = 0$, which now

¹⁵Although in the model of [14] the scalar is complex (it carries lepton number), from the point of view of the potential for the real part of s , it reduces to our case.

have very simple expressions:

$$\begin{aligned} \frac{\partial V}{\partial h} = 0 &\Rightarrow \left\{ h = 0, \quad \text{and} \quad h^2 = D_h^2(s) = \frac{1}{2\lambda_h}(2\mu_h^2 - \lambda_m s^2) \right\}, \\ \frac{\partial V}{\partial s} = 0 &\Rightarrow \left\{ s = 0, \quad \text{and} \quad h^2 = D_s^2(s) = -\frac{2}{\lambda_m}(\mu_s^2 + \lambda_s s^2) \right\}. \end{aligned} \quad (4.5)$$

That is, now $D_h^2(s)$ and $D_s^2(s)$ are just parabolas with the same axis of symmetry, at $s = 0$, and different widths¹⁶. Furthermore, to understand the nature of stationary points along the branch $s = 0$, it is useful to write

$$\left. \frac{\partial^2 V}{(\partial s)^2} \right|_{s=0} = \frac{1}{2}\lambda_m[h^2 - \bar{h}_s^2]. \quad (4.6)$$

meaning that, for $\lambda_m > 0$ ($\lambda_m < 0$) minima along $s = 0$ can only appear for h^2 above (below) the vertex $\bar{h}_s^2 = -2\mu_s^2/\lambda_m$ of the $D_s^2(s)$ parabola.

Can this constrained setting give rise to a tree-level barrier? As we saw in the previous Section, in order to arrange for two degenerate minima, one at $h = 0$ and the other at $h \neq 0$, no tree-level barrier can appear if the broken minimum has $w \neq 0$. This is because the \mathbf{Z}_2 -symmetry enforces the existence of two minima with $s = \pm w$ but this prohibits a minimum at $h = 0$, as discussed below eq. (2.29).¹⁷ Hence, the \mathbf{Z}_2 -symmetric case can only have a tree level barrier at the critical temperature if the minimum with $h^2 > 0$ lies at the symmetry axis $w = w_p = 0$. This situation is illustrated by Fig. 4 which shows the intersecting curves $D_{h,s}^2(s)$ in the $(h^2/v^2, s/w_0)$ -plane (left plot) and the corresponding potential with its barrier (right plot). We focus on this particular case in the rest of this Section.

Following the approach of Section 2, we identify the conditions for a barrier separating the broken and unbroken minima. From eq. (2.29), we know that along $h = 0$, stable minima $(0, \pm w_0)$ require $D_h^2(w_0) < 0$ which leads to

$$\lambda^2 < -\frac{\lambda_m m_s^2}{2v^2} < 0, \quad \lambda_m > 0, \quad (4.7)$$

where w_0 , solution of $D_s^2(w_0) = 0$, is given by

$$w_0^2 = -\frac{\mu_s^2}{\lambda_s} = \frac{m_h^2(\lambda_m v^2 - 2m_s^2)}{v^2(4\lambda^2 + \lambda_m^2)}. \quad (4.8)$$

Furthermore, the condition of degeneracy, eq. (2.43), imposes

$$\lambda^2 = \frac{m_s^4 - \lambda_m v^2 m_s^2}{v^4}. \quad (4.9)$$

¹⁶Which parabola is widest depends on the relative size of the two widths $\lambda_m/(2\lambda_h)$ vs. $2\lambda_s/\lambda_m$ and is therefore controlled by the sign of λ^2 .

¹⁷In terms of the two parabolas $D_{h,s}^2(s)$, it is difficult to arrange that they cut twice, at the broken minimum and at the saddle point in between, because they have the same axis of symmetry, at $s = 0$.

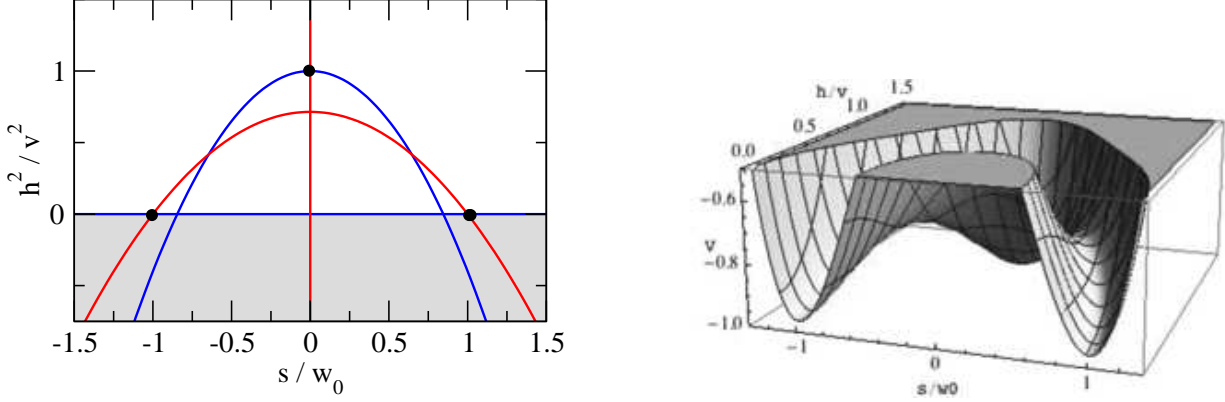


Figure 4: Special scenario with \mathbf{Z}_2 symmetry, $\lambda_m > 0$ and $\lambda^2 < 0$. Left, curves with $\partial V/\partial h = 0$ [$D_h^2(s)$ and $h = 0$, blue lines] and $\partial V/\partial s = 0$ [$D_s^2(s)$ and $s = 0$, red lines] intersecting in the minima at $(0, \pm w_0)$ and $(v, 0)$, as indicated by the black dots. Right, corresponding potential showing the barrier between minima.

This condition can be rewritten as

$$m_s^2 = \frac{v^2}{2} \left(\lambda_m - 2\sqrt{\lambda_h \lambda_s} \right), \quad (4.10)$$

which will be useful later on.

In this degenerate case, the potential then takes the form

$$V = \frac{1}{8} m_h^2 v^2 \left[4 \frac{R_s}{R_h} \frac{h^2 s^2}{v^2 w_0^2} + \left(\frac{h^2}{v^2} + \frac{s^2}{w_0^2} - 1 \right)^2 \right], \quad (4.11)$$

showing a concrete example in which the overall shape of the potential is controlled by the ratio R_s/R_h . This is now the only relevant shape parameter (as was to be expected starting with only 5 d.o.f.s and removing 3 for rescalings, 1 for degeneracy and no shift freedom) and it controls the height of the barrier that separates the symmetric and broken minima. For comparison with other cases, notice that this degenerate \mathbf{Z}_2 scenario corresponds in fact to the shape parameters $\lambda_m/R_h = 1 + 2R_s/R_h$ and $R_{sh}/R_h = 0$.

4.0.1 Case with Flat Directions

Applying the general discussion of flat directions in Section 2 to the particular case of the \mathbf{Z}_2 -symmetric scenario, we see that a flat direction arises for

$$\frac{\mu_h^2}{\lambda_h} = -\frac{2\mu_s^2}{\lambda_m}, \quad \lambda^2 = \lambda_h \lambda_s - \frac{1}{4} \lambda_m^2 = 0. \quad (4.12)$$

If this happens, then the tree-level potential takes the simple form

$$V = -\frac{1}{2} \mu_h^2 \left(h^2 + \frac{1}{2} \frac{\lambda_m}{\lambda_h} s^2 \right) + \frac{1}{4} \lambda_h \left(h^2 + \frac{1}{2} \frac{\lambda_m}{\lambda_h} s^2 \right)^2. \quad (4.13)$$

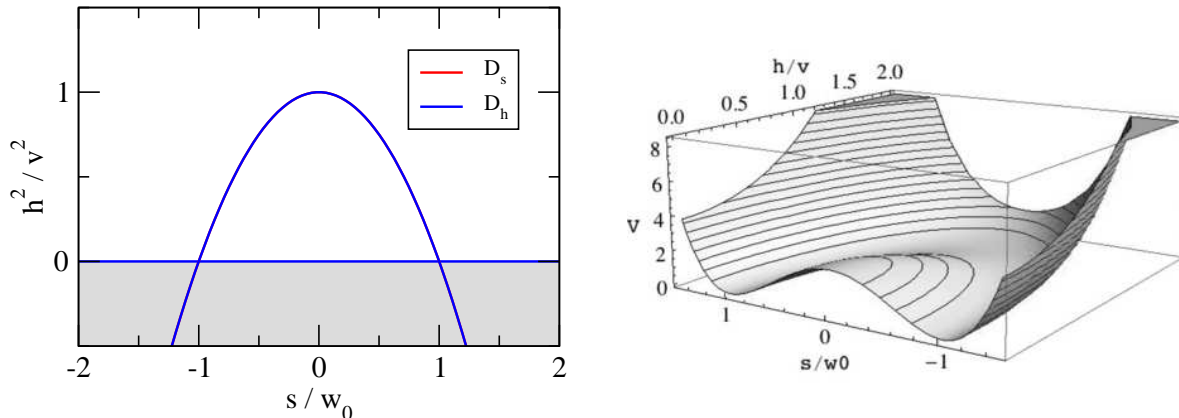


Figure 5: Special scenario with \mathbf{Z}_2 symmetry, $\lambda_m > 0$ and $\lambda^2 = 0$ showing a flat direction. Left, degenerate parabolas $D_{h,s}^2(s)$. Right, corresponding potential.

When thinking about further possible symmetries that could enforce such form of the potential one should keep in mind that this form is supposed to hold at some critical temperature, not at $T = 0$. While the symmetric form of the quartic couplings would be approximately respected by thermal corrections (as quartics have only a logarithmic dependence on T), quadratic terms for h and s do evolve differently with temperature and would break that symmetry. We will examine this in more detail in the next Subsection.

There are two qualitatively-different cases depending on the sign of λ_m . (The limiting case $\lambda_m = 0$ has little interest, as then s and h are completely decoupled from each other.) For $\lambda_m > 0$, the flat direction is the parabola

$$h^2 + \frac{1}{2} \frac{\lambda_m}{\lambda_h} s^2 = \frac{\mu_h^2}{\lambda_h}, \quad (4.14)$$

closed around the origin. Then the potential looks like a Mexican-hat potential, see Fig. 5. Of course such potential would not be acceptable at $T = 0$ (implying in particular a massless scalar) but could be of interest at $T = T_c$: the effect of the thermal cubic from gauge bosons can be enhanced by the flatness of the potential, leading to a large $v(T_c)/T_c$. This is confirmed by our numerical analysis. As we will see below, when T falls below T_c the minimum (which at $T = T_c$ is not located at any precise point along the flat direction) will be driven either to $h = 0, s \neq 0$ (a case which does not interest us) or to $h \neq 0, s = 0$, with a big jump in $v(T_c)/T_c$.

For $\lambda_m < 0$, the degenerate parabolas correspond to two flat directions

$$h^2 - \frac{1}{2} \frac{|\lambda_m|}{\lambda_h} s^2 = \frac{\mu_h^2}{\lambda_h}, \quad (4.15)$$

running away to infinity, see Fig. 6. The stability of the potential along such directions

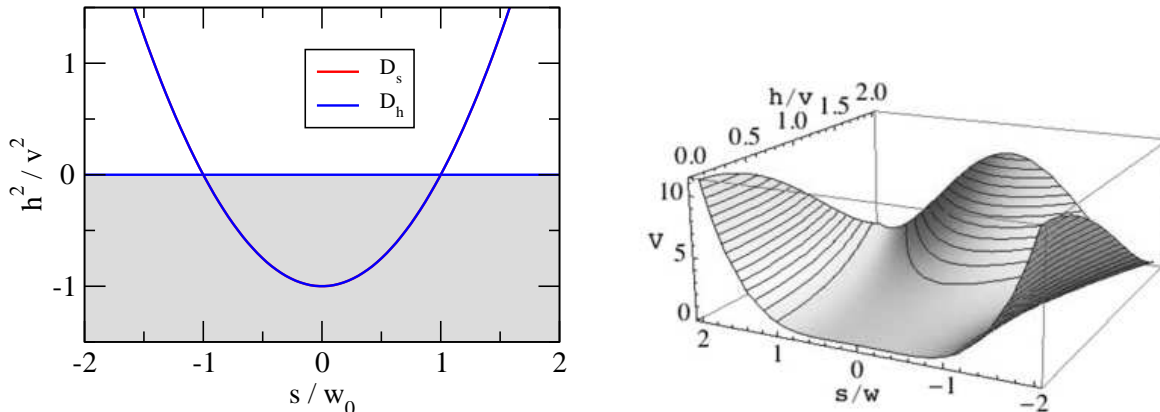


Figure 6: Special scenario with \mathbf{Z}_2 symmetry, $\lambda_m < 0$ and $\lambda^2 = 0$ showing two flat directions. Left, degenerate parabolas $D_{h,s}^2(s)$. Right, corresponding potential.

should be ensured by mass terms or one-loop quartics. This case could be of interest for the transition if the flat directions intersect $h = 0$, which requires $\mu_h^2 < 0$. The thermal evolution of the potential in this case will depend crucially on the thermal cubic.

4.1 Thermal Evolution and EW Phase Transition

As we saw in Section 3, at leading order in the high- T expansion, only μ_s^2 and μ_h^2 are affected, according to eqs. (3.3).¹⁸ As a result, when T is lowered from T_c down to $T = 0$, the parabolas $D_h^2(s)$ and $D_s^2(s)$ simply drift away from $h = 0$ keeping their width and symmetry axis fixed. As they move at different rates, determined by [see eq. (3.4)]

$$\frac{dD_h^2(s)}{dT^2} = -\frac{c_h}{\lambda_h}, \quad \frac{dD_s^2(s)}{dT} = -\frac{2c_s}{\lambda_m}, \quad (4.16)$$

their relative position can change, together with the location of the minima in the potential. This is illustrated by Fig. 7, which shows snapshots of $D_{h,s}^2(s)$ at different temperatures. At very high T the minimum is at $(0, 0)$. The \mathbf{Z}_2 symmetry breaks spontaneously at some critical temperature T_Z and the two minima at $(0, \pm w_0(T))$ move away from the origin as T gets lower. Eventually the EW minimum forms and gets degenerate with the \mathbf{Z}_2 -breaking minima at T_c . For lower temperatures, the EW minimum is the deepest one.

Let us focus on cases that lead to a tree-level barrier, which, as explained above, require $w = 0$, $\lambda_m > 0$ and $\lambda^2 < 0$. Once we identify the parameters that give such barrier in the

¹⁸ Note that, in the context of the Singlet Majoron Model, right-handed neutrino Yukawas give a significant contribution to c_s and the imaginary component of the (complex) singlet contributes to both c_s and c_h , increasing the coefficients of λ_s and λ_m in (3.2).

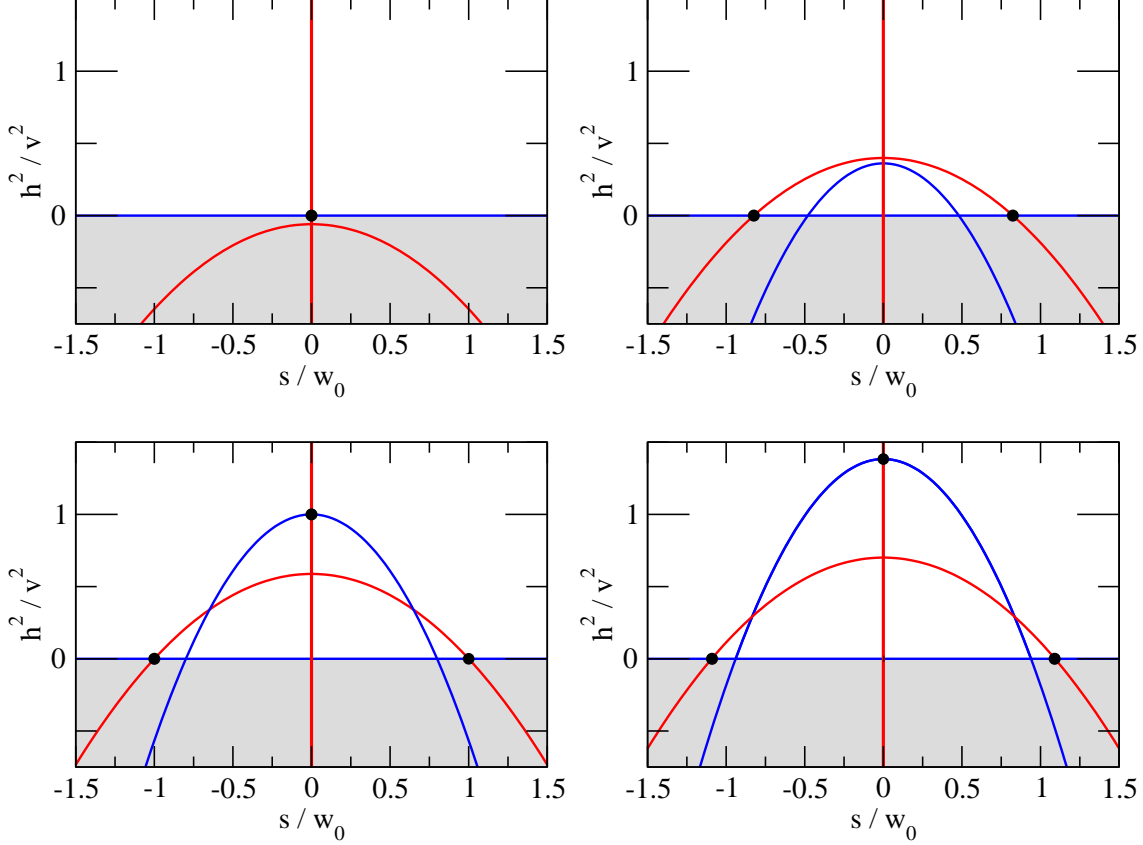


Figure 7: Snapshots of the T -dependent curves $D_h^2(s)$ (blue lines) and $D_s^2(s)$ (red lines) intersecting at the T -dependent minima (black dots) in a \mathbf{Z}_2 -symmetric scenario with the correct cosmological history. The plots are in order of decreasing T , from left to right and top to bottom, with $T \gtrsim T_Z$ (upper left); $T_Z > T > T_c$ (upper right); $T = T_c$ (lower left); and $T = T_c/2$ (lower right).

potential, $V_c(h, s)$, of the form (4.11), we still have the freedom to choose T_c and to perform the appropriate rescaling to ensure $v(0) = v_{EW}$. To be specific, the potential is

$$V = V_c(h, s) - \frac{1}{2}(T_c^2 - T^2)(c_h h^2 + c_s s^2). \quad (4.17)$$

As explained in Section 3, we start at T_c with degenerate minima with broken and unbroken EW symmetry: $V_b(T_c) = V_s(T_c)$. As T is lowered we want that the broken minimum gets deeper becoming our vacuum, in which case, $w(T)$ will stay at zero for all $T < T_c$. One has

$$\Delta V_{bs}(T) = V[v(T), 0] - V[0, w_0(T)] = -\frac{\mu_h^4(T)}{4\lambda_h} + \frac{\mu_s^4(T)}{4\lambda_s}, \quad (4.18)$$

so, to end up at the broken minimum at $T = 0$ we need the condition¹⁹

$$\frac{c_h}{c_s} > \sqrt{\frac{\lambda_h}{\lambda_s}} = \frac{w_0^2}{v^2} , \quad (4.19)$$

which can be taken as a constraint on the initial parameters v and w_0 in a specific model where c_h and c_s are known constants. Alternatively, we can separate from c_s its λ_s -dependent part [see (3.2)] as

$$c_s = \frac{1}{4}\lambda_s + \delta c_s , \quad (4.20)$$

where $\delta c_s = \lambda_m/6$ here, but in general can include contributions from other particles coupled to the singlet. Then, condition (4.19) translates into a lower limit on λ_s :

$$\lambda_s > \lambda_{s,min} \equiv \frac{4}{\lambda_h} \left[2c_h^2 - \lambda_h \delta c_s - 2c_h \sqrt{c_h^2 - \lambda_h \delta c_s} \right] , \quad (4.21)$$

while an upper limit follows from eq. (4.7):

$$\lambda_s < \lambda_{s,max} \equiv \frac{\lambda_m^2}{4\lambda_h} . \quad (4.22)$$

Obviously, $\lambda_{s,min} < \lambda_{s,max}$ should be satisfied.

The T -dependence of our parametrization is as follows. In the approximation we work, quartic couplings do not depend on the temperature while the rest of parameters do depend on it, leading to $m_h^2(T)$, $m_s^2(T)$ and $v(T)$. This T -dependence can be extracted from eqs. (2.7)-(2.13), after feeding in them the T -dependent μ_h^2 and μ_s^2 . In this way it is straightforward to extract

$$v^2(T) = v_{EW}^2 - \frac{c_h}{\lambda_h} T^2 , \quad (4.23)$$

where we are always implicitly assuming $T < T_c$ (so that the EW minimum is the global one) which is the range of interest to run parameters from T_c down to $T = 0$. From this we can already extract the important ratio $v(T_c)/T_c$ as

$$\frac{v(T_c)}{T_c} = \sqrt{\frac{v_{EW}^2}{T_c^2} - \frac{c_h}{\lambda_h}} . \quad (4.24)$$

Notice, however, that the phase transition cannot be made arbitrarily strong by choosing low T_c , in which case $v(T_c) \simeq v_{EW}$, since then the tunneling probability becomes small and the meta-stable symmetric phase will become stable. Moreover, for low T_c the high- T approximation breaks down.

¹⁹In this simple scenario, this condition coincides with the condition derived from $d\Delta V_{bs}(T)/dT^2 = [c_h v^2 - c_s w_0^2]/2 > 0$, see the discussion around eq. (3.7).

Eq. (4.24) becomes more meaningful when combined with information on the mass spectrum. For the Higgs mass parameter we have

$$m_h^2(T) = 2\lambda_h v^2(T) , \quad (4.25)$$

where the physical value of the Higgs mass $M_h^2 = m_h^2(0)$ fixes λ_h through $M_h^2 = 2\lambda_h v_{EW}^2$ [here we use capital letters for the $T = 0$ parameters: $M_h^2 \equiv m_h^2(0)$ and $M_s^2 \equiv m_s^2(0)$]. Similarly, the singlet mass is given by

$$m_s^2(T) = m_s^2 + \left(\frac{\lambda_m}{2\lambda_h} c_h - c_s \right) (T_c^2 - T^2) . \quad (4.26)$$

Notice that the second term is positive for $T < T_c$ due to $\lambda_h \lambda_s < \lambda_m^2/4$ and eq. (4.19), such that the zero temperature mass of the singlet is larger than the one at the critical temperature: $M_s^2 > m_s^2$. From the condition of degenerate minima, eq. (4.10), we can obtain the additional relation

$$m_s^2 = \frac{1}{2} v^2(T_c) (\lambda_m - 2\sqrt{\lambda_h \lambda_s}) , \quad (4.27)$$

arriving at

$$M_s^2 = \frac{1}{2} \left(\lambda_m - 2\sqrt{\lambda_h \lambda_s} \right) v_{EW}^2 + \left(c_h \sqrt{\frac{\lambda_s}{\lambda_h}} - c_s \right) T_c^2 . \quad (4.28)$$

So, the singlet mass squared is a simple linear combination of the two mass scales v_{EW}^2 and T_c^2 with positive coefficients. For $\lambda_s = \lambda_{s,min}$, the coefficient of T_c^2 in eq. (4.28) is zero and M_s is independent of T_c . In the case $\lambda_s = \lambda_m^2/(4\lambda_h)$ it is the coefficient of v_{EW}^2 that cancels, and then M_s increases linearly with T_c . This is precisely the limiting case with a flat direction at T_c (of $\lambda_m > 0$ type) discussed in the previous Subsection.

To explore in more detail what masses and $v(T_c)/T_c$ are allowed we will proceed as follows. Cases with a barrier are simply found by choosing $\lambda_m > 0$ and $-\lambda^2$ in the interval $(0, \lambda_m^2/4)$, which in terms of λ_s is equivalent to $\lambda_s \in (0, \lambda_{s,max})$. The lower part of this interval is removed by the condition (4.21), required to guarantee the correct $T \rightarrow 0$ limit, leaving only the interval $(\lambda_{s,min}, \lambda_{s,max})$. Now, for fixed M_h and using T_c as a parameter, we can obtain $v(T_c)/T_c$ and M_s for different choices of λ_m and λ_s in the appropriate ranges described above. The results are as shown in Fig. 8, which presents three representative cases: *a)* $M_h = 115$ GeV with $\lambda_m = 0.2$ and then $\lambda_s \in (0.03, 0.09)$; *b)* $M_h = 115$ GeV with $\lambda_m = 1$ and $\lambda_s \in (0.09, 2.29)$; and *c)* $M_h = 200$ GeV with $\lambda_m = 0.5$ and $\lambda_s \in (0.09, 0.19)$. In the upper plot, we show the large value of $v(T_c)/T_c$ (which is independent of λ_s) that can be obtained as a function of T_c . For $v(T_c)/T_c \gtrsim 4$ we cannot trust the high- T approximation, so we do not explore smaller values of T_c . In the rest of the plots we show the value of the singlet scalar mass M_s as a function of the critical temperature T_c for equally spaced

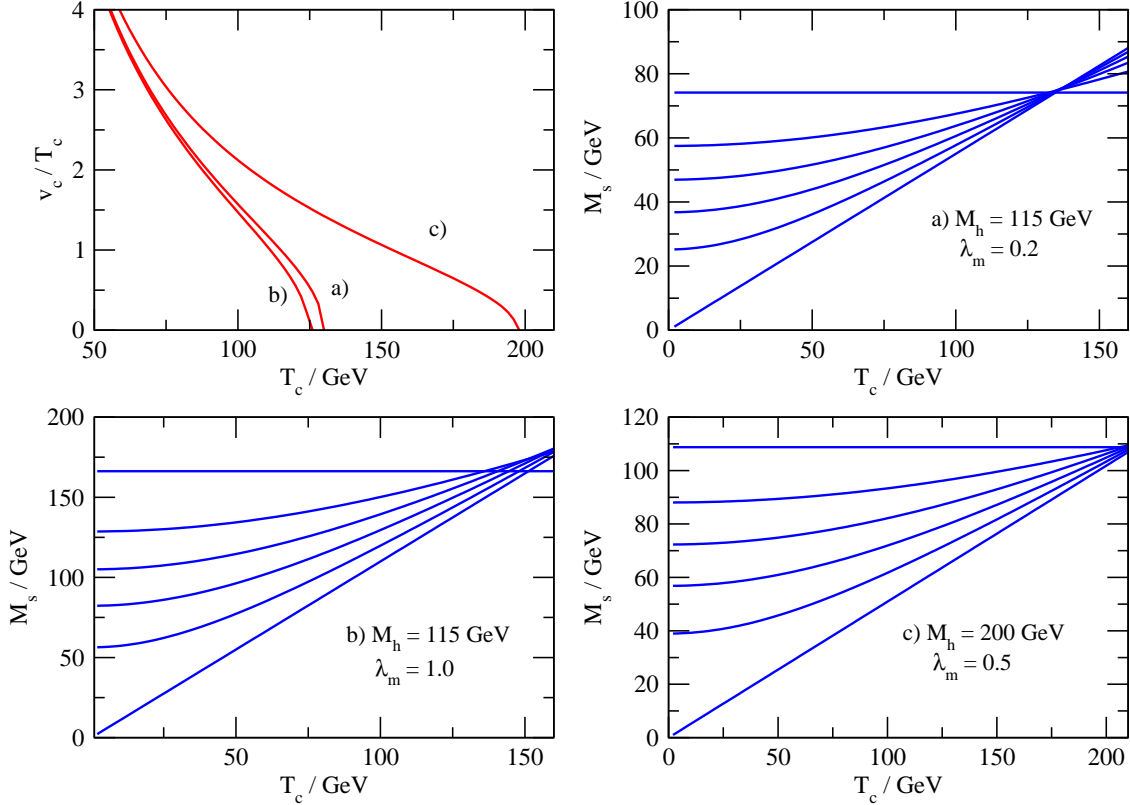


Figure 8: Ratio $v(T_c)/T_c$ (upper-left plot) and values of the singlet scalar mass (rest of plots) as a function of the critical temperature for the cases a) $M_h = 115$ GeV, $\lambda_m = 0.2$; b) $M_h = 115$ GeV, $\lambda_m = 1$; c) $M_h = 200$ GeV and $\lambda_m = 0.5$. Different masses correspond to different values of $\lambda_s \in (\lambda_{s,min}, \lambda_{s,max})$, with M_s increasing for lower λ_s .

values of $\lambda_s \in (\lambda_{s,min}, \lambda_{s,max})$. Higher singlet masses correspond to lower values of λ_s . One concludes that very strong first-order EW transitions can be obtained for a wide range of scalar masses.

4.2 One-loop Numerical Analysis

So far, we have identified choices for the $T = 0$ parameters that lead to strong electroweak phase transitions in the mean-field approximation. It is straightforward to refine these results starting from the same tree-level parameters but including in the scalar potential one-loop $T = 0$ corrections and the full one-loop thermal integrals (which correctly take into account Boltzmann decoupling effects) further improved by daisy resummation. Details of this standard procedure are given in Appendix A. To illustrate the impact of this refinement, we show in Fig. 9 the ratio v_c/T_c in the mean-field approximation (blue dashed line) compared with

the same quantity calculated with the one-loop thermal potential just described (black solid line). The example shown corresponds to $M_h = 115$ GeV and $M_s = 145$ GeV. As expected from the correct inclusion of Boltzmann decoupling effects, which tend to increase T_c (see inset, where $T_{c,MF}$ corresponds to the critical temperature in the mean-field approximation, while $T_{c,1L}$ takes into account the full one-loop resummed potential), the one-loop transition is weaker²⁰ than in the mean-field approximation but still strong enough to allow for baryogenesis.

We have also examined at one-loop cases with a flat direction with $\lambda_m > 0$, case in which thermal cubics from bosons play an important role. Although such thermal effects would not give rise to strong transitions by themselves (for weak couplings to the Higgs field), in the presence of a flat direction the thermal cubic lifts the flat direction creating a barrier between the broken and symmetric minima, and ensures large jump in $v(T)/T$, leading to strong phase transitions at one-loop. Concerning the naturalness of such scenario, notice that all that is required to realize it is that quartic couplings satisfy $\lambda^2 = 0$ (which might be the result of some symmetry). This makes the parabolas $D_h^2(s)$ and $D_s^2(s)$ equally wide and, as they are both centered at $s = 0$, when they shift with temperature, it is guaranteed that they will overlap and give a flat direction at some T_c .

Our results contradict some claims in the literature concerning this scenario [37], which were focused on transitions driven by the thermal cubic. On the other hand, the analysis of the Singlet Majoron model in [14] did find strong transitions. One important difference between that study and ours is that, for phenomenological reasons (in particular to be able to generate nonzero neutrino masses), the scenarios considered in [14]²¹ are restricted to $w \neq 0$, which works against the possibility of obtaining a really strong phase transition through tree-level barriers. However, loop effects related to sizable Yukawa couplings (to the right-handed neutrinos), that we are not discussing, can help in getting strong EWPhTs. On the other hand, it is clear that the example in Fig. 9 of [14] corresponds to a one-loop deformation of a tree-level case with a nearly flat direction. One-loop effects shift the EW minimum away from $w = 0$ and lead to a very light scalar, see eq. 4.3.

²⁰When comparing the two curves in Fig. 9, keep in mind that, for a given choice of the model parameters, the resulting $v(T_c)/T_c$ at one-loop is displaced to higher T_c and lower $v(T_c)/T_c$ with respect to the tree-level value (like the curves' end-points demonstrate).

²¹A direct comparison of results is difficult because the analysis in [14] is based on scans of the parameter space (for instance, from distributions of λ_h, λ_s and λ_m we cannot obtain the distribution of λ^2 , which is a crucial parameter for EWPhTs) and different mechanisms operate in different regions of parameter space.

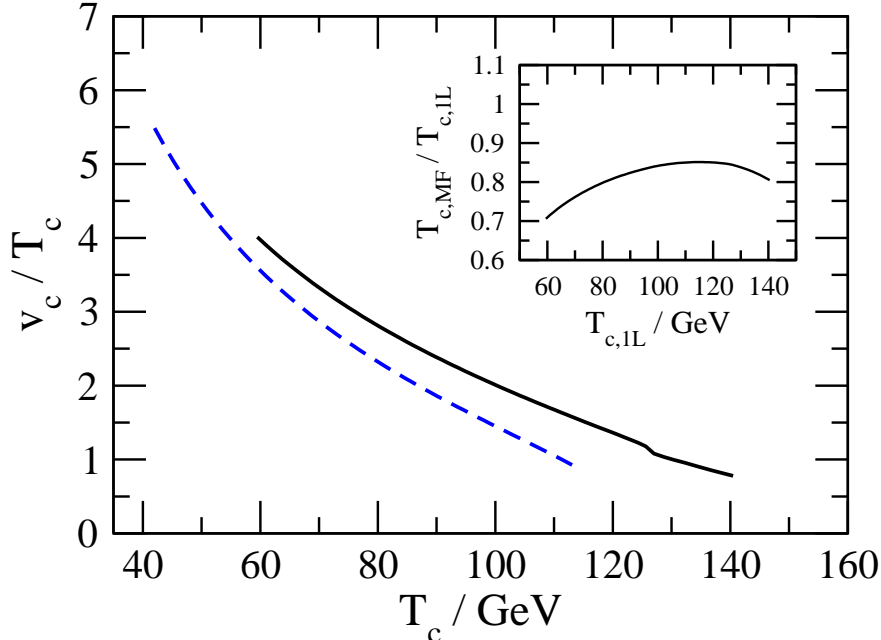


Figure 9: The ratio v_c/T_c in the mean-field approximation (blue dashed line) and the one-loop approximation (black solid line) as a function of the corresponding critical T_c . The relation between critical temperatures in the two approximations is shown in the inset. Here $M_h = 115$ GeV, $M_s = 145$ GeV and $w_0 = 100$ GeV. $T_{c,MF}$ corresponds to the critical temperature in the mean-field approximation, while $T_{c,1L}$ takes into account the full one-loop resummed potential.

5 Special Cases: A Supersymmetric Example

A different context in which a particular region of parameter space is selected by some mechanism, is that of supersymmetry. A supersymmetric version of the SM plus singlet model, the Next to Minimal Supersymmetric Standard Model (NMSSM), has been considered since long ago as suitable to obtain a strong electroweak phase transition with applications to electroweak baryogenesis. In particular, ref. [48] was the first to emphasize in this context the relevance of a tree-level cubic term in the scalar potential.

Here we will examine a particular deformation of this model, the near-to-Minimal Supersymmetric Standard Model (nMSSM) [49], which differs from the NMSSM in having a singlet superpotential with a loop-suppressed tadpole and no cubic term. Refs. [16] studied the electroweak phase transition in this model finding strongly first-order cases. In the region of parameter space examined in [16] the scalar potential reduces to that of a SM Higgs plus

a real scalar with a potential of our general form (2.1) but with

$$\lambda_s = 0, \quad \mu_3 = 0, \quad \lambda_m > 0. \quad (5.1)$$

It is interesting to note that a shift of the singlet respects the conditions $\mu_3 = 0$ and $\lambda_s = 0$ so that there is freedom to set $\mu_m = 0$ without loss of generality. In terms of the parameters of eqs. (2.7)-(2.13) these conditions read

$$\lambda^2 = -\frac{\lambda_m^2}{4}, \quad m_* = -\frac{\lambda_m^2}{4}w, \quad m_{sh}^2 = \lambda_m v w \quad (5.2)$$

and the model can be described by just 5 parameters,

$$\{v, w, m_h^2, m_s^2, \lambda_m\}. \quad (5.3)$$

The model has sufficient structure in the $D_{h,s}^2(s)$ functions to allow for tree-level barriers, which must necessarily be of type-(d) in the classification of eqs. (2.37)-(2.40), that is, of those with $\lambda_m > 0$ (imposed by supersymmetry) and $(w_0 - w_p)(w - w_p) > 0$. This last condition can be explicitly checked after translating the conditions of eq. (5.1) into the parameters for a degenerate minimum (see Table 1) or, equivalently, imposing the parameter constraints needed to have a symmetric minimum at $(0, w_0)$ degenerate with the broken one at (v, w) , which now read:

$$w_0 = w + \frac{m_h^2 v^2}{8m_s^2 w} \left[1 + \sqrt{1 + \left(4 \frac{m_s w}{m_h v}\right)^2} \right], \quad \lambda_m = \frac{m_h^2}{w^2} \left[-1 + \sqrt{1 + \left(4 \frac{m_s w}{m_h v}\right)^2} \right], \quad (5.4)$$

and $w_p = 0$, from which one gets $(w_0 - w_p)(w - w_p) = w w_0$, which is always positive. Fig. 10 shows an example of such barrier.

The potential with degenerate vacua takes the simple form

$$V = \frac{1}{8} v^2 m_h^2 \left[\left(\frac{h^2}{v^2} + \frac{s-w}{w_0} - 1 \right)^2 + \left(4 \frac{R_s}{R_h} - 1 \right) \frac{h^2 (s-w)^2}{v^2 w_0^2} \right], \quad (5.5)$$

where we have one single shape parameter: R_s/R_h , as in the \mathbf{Z}_2 -symmetric scenario, but now with $\lambda_m/R_h = 2R_s/R_h - 1/2$ and $R_{sh}/R_h = 1/2$. In the particular case $4R_s/R_h = 1$ the potential (5.5) develops a flat direction which, in the $(h^2/v^2, s/w_0)$ -plane, is a straight line through both minima. In terms of the original quartic couplings of the potential this scenario corresponds to the extreme limit $\lambda_m = 0$, that we do not consider further.

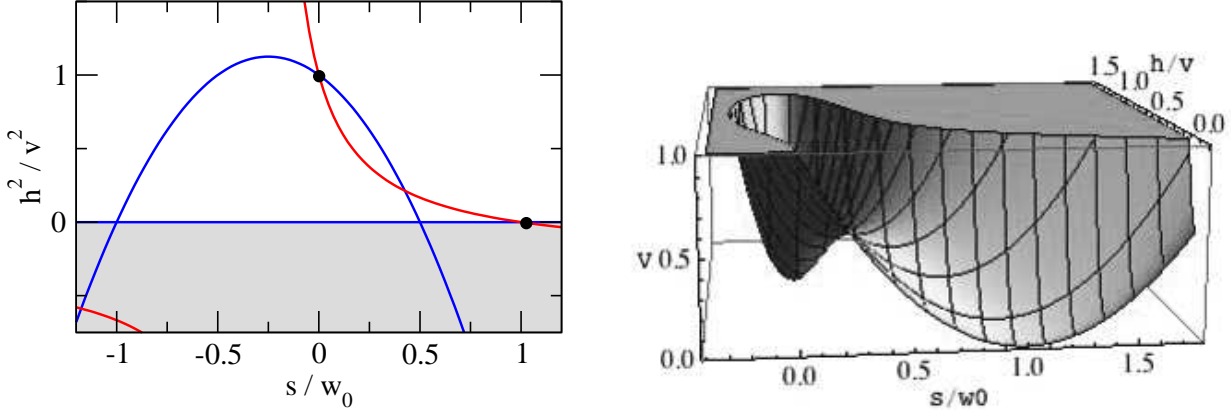


Figure 10: Scenario with a strong transition in the nMSSM model. Left, intersecting curves $D_{h,s}^2(s)$. Right, corresponding potential.

5.1 Thermal Evolution and EW Phase Transition

As in previous scenarios, we start from the potential with degenerate minima, which is assumed to hold at some T_c , and then use the mean-field approximation to derive the corresponding potential parameters at $T = 0$. This temperature evolution is given in eq. (3.3) where now the constants c_h , c_s and m_3 will also receive contributions from supersymmetric particles (if their masses are not much higher than T). As the model can support a strong electroweak phase transition without the need of supersymmetric particles coupled sizeably to the Higgs (as needed in the MSSM case) we simplify the analysis by assuming that thermal effects from superpartners are Boltzmann suppressed. If supersymmetric particles do not decouple from the thermal plasma their effects can be included and they will only modify quantitatively our discussion of strong phase transitions based on the tree-level potential.

Note that the condition $\mu_m = 0$, that we have previously imposed using the shift symmetry, is respected by thermal corrections (in the mean-field approximation) and implies that $D_h^2(s)$ is centered at $w_p = 0$ and has the same width at all T 's while its vertex \bar{h} will evolve with T as in the \mathbf{Z}_2 case. Another good property of this choice is that $m_3 = 0$, see (3.2), so that μ_1^3 is also T -independent. This makes the evolution of $D_s^2(s)$ also very simple:

$$\frac{D_s^2(s)}{dT^2} = -\frac{2c_s}{\lambda_m}, \quad (5.6)$$

exactly as in the \mathbf{Z}_2 case, so that also $D_s^2(s)$ keeps its shape and simply drifts. As usual, to have a successful cosmological history, $D_{h,s}^2(s)$ should move in such a way that the EW vacuum forms and gets deeper at low temperature.

The thermal evolution of the potential minimum in this model is more complicated than

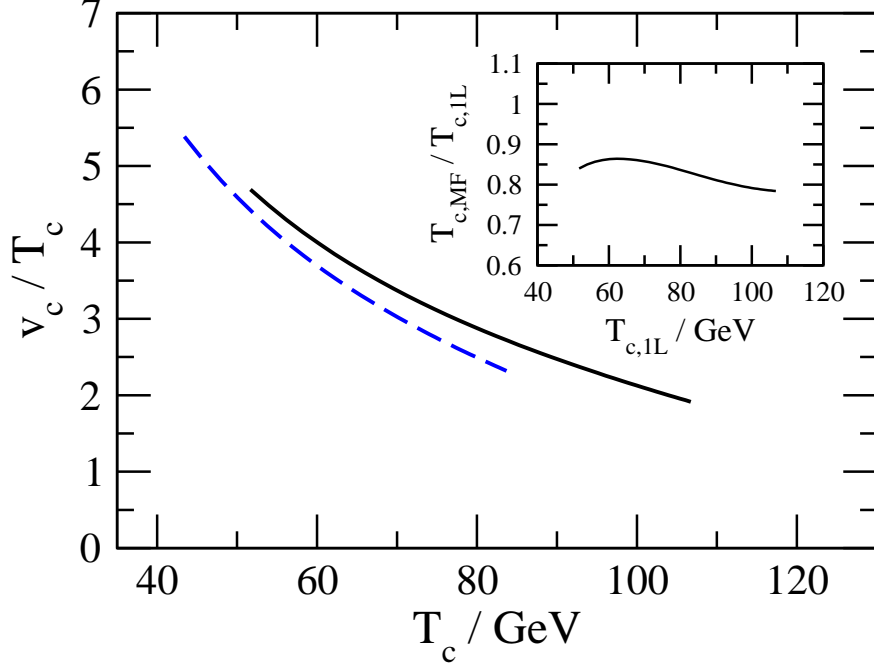


Figure 11: The ratio v_c/T_c in a nMSSM scenario in the one-loop approximation (black solid line) as a function of the corresponding critical T_c . The relation between critical temperatures in the two approximations is shown in the inset. Here $M_h = 135$ GeV, $M_s = 145$ GeV and $w_0 = -400$ GeV.

in the \mathbf{Z}_2 symmetric case: $v(T)$, $w(T)$ and $m_s(T)$ are determined by the simple equations:

$$\mu_h^2(0) - c_h T^2 = \lambda_h v^2(T) + \frac{1}{2} \lambda_m w^2(T) , \quad (5.7)$$

$$\mu_s^2(0) + c_s T^2 = m_s^2(T) - \frac{1}{2} \lambda_m v^2(T) , \quad (5.8)$$

$$\mu_1^3 = -m_s^2(T)w(T) = \mu_s^2(T)w_0(T) , \quad (5.9)$$

while $m_h^2(T)$ is trivially related to $v(T)$ by $m_h^2(T) = 2\lambda_h v^2(T)$, as usual. This system of equations can be solved analytically, although the resulting expressions for $v^2(T)$, $w(T)$ and $m_s^2(T)$, being solutions of cubic equations, are not very illuminating and we refrain from writing them down.

Once the temperature dependence of all parameters is known, we can relate the parameters at the critical temperature

$$\{v, w, m_h^2, m_s^2, \lambda_m\} \quad (5.10)$$

to those at zero temperature

$$\{v_{EW}, w_{EW}, M_h^2, M_s^2, \lambda_m\} \quad (5.11)$$

and, in particular, determine the critical temperature in terms of the physical parameters. Some simple relations are

$$\begin{aligned}
M_h^2 &= m_h^2 \frac{v_{EW}^2}{v^2} , \\
M_s^2 &= m_s^2 \frac{w}{w_{EW}} , \\
M_s^2 - m_s^2 &= \frac{1}{2} \lambda_m (v_{EW}^2 - v^2) - c_s T_c^2 .
\end{aligned}
\tag{5.12}$$

Once we have the $T = 0$ potential we can perform a refined one-loop analysis including thermal decoupling effects as already discussed in previous Sections to confirm the existence of strong phase transitions in the regions indicated by the tree-level analysis. An example of the results we obtain is given in Fig. 11.

6 Special Cases: Light Scalar

As a final example we consider a realization of the SM plus a singlet with a very light scalar, put forward in [41] as a possible way of increasing the strength of the EWPhT. The model has

$$\lambda_m = 0 , \quad \mu_1 = 0 , \quad \mu_3 = 0 , \quad \lambda_s = 0 ,
\tag{6.1}$$

and μ_m , the only coupling connecting the s and h sectors, is small: $\mu_m \equiv \epsilon_m v_{EW} \ll v_{EW}$. The condition $\mu_1 = 0$ is not respected by thermal corrections and therefore we have to keep it nonzero in our discussion, but with $\mu_1(0) = 0$. In our parametrization this reads

$$\lambda_m = 0 , \quad \lambda^2 = 0 , \quad m_* = 0 .
\tag{6.2}$$

This case has only five free parameters that we can take as $\{v, w, m_h^2, m_s^2, \mu_m\}$. So, this is a very constrained scenario and one sees (cf. Table 1) that the conditions (2.46)-(2.47) cannot be fulfilled: it is not possible to have degenerate minima with a barrier in between. This can be easily understood by studying the functions $D_{h,s}^2(s)$, which are straight lines now:

$$D_h^2(s) = \frac{1}{2\lambda_h} (2\mu_h^2 - \mu_m s) ,
\tag{6.3}$$

$$D_s^2(s) = -4 \frac{\mu_1^3 + \mu_s^2 s}{\mu_m} ,
\tag{6.4}$$

and, with such simple structure, cannot lead to a tree-level barrier unless a scenario with a flat direction (or close to it) is realized. Such flat direction requires $\mu_m \mu_h^2 = -4\lambda_h \mu_1^3$ and $\mu_m^2 = 8\lambda_h \mu_s^2$. To decide how natural this is, we need to examine the thermal evolution of these quantities.

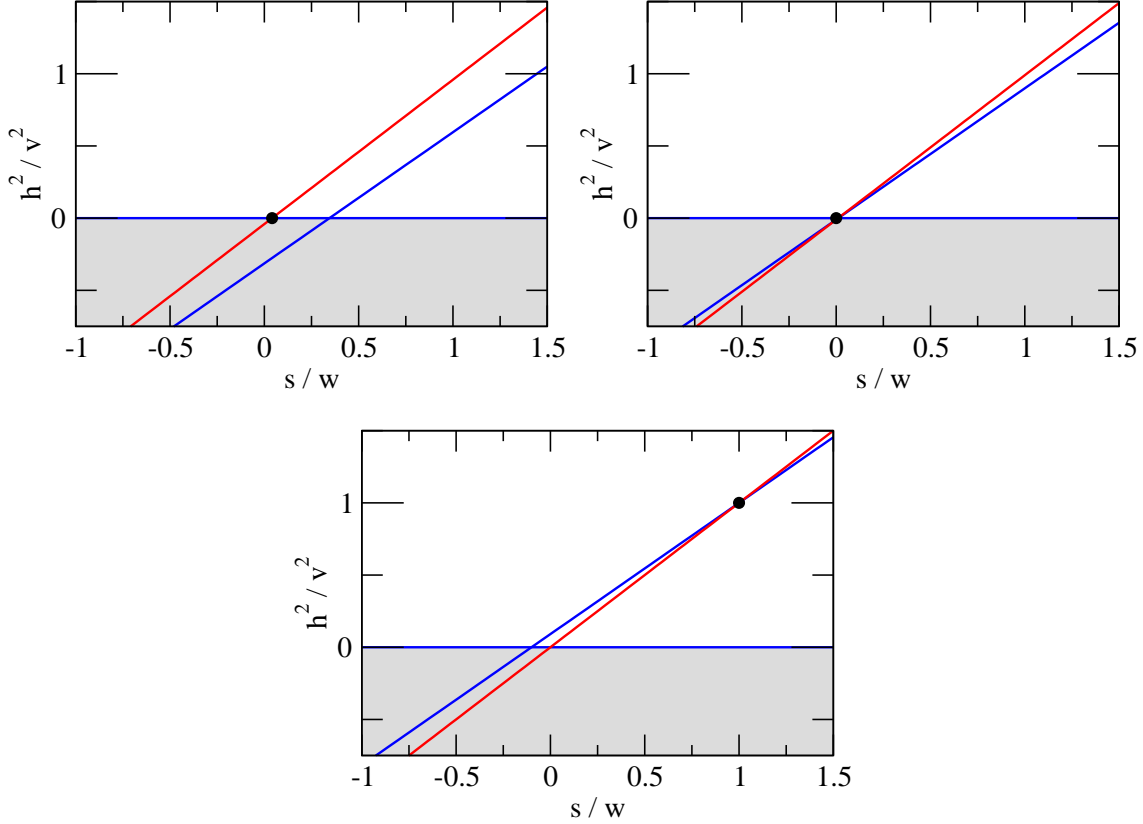


Figure 12: Snapshots of the T -dependent lines $D_h^2(s)$ (blue) and $D_s^2(s)$ (red) intersecting at the T -dependent minimum (black dot) in a scenario with a light singlet having the correct cosmological history. The plots are in order of decreasing T , from left to right and top to bottom, with $T > T_c$ (upper left); $T = T_c$ (upper right); and $T < T_c$ (bottom).

6.1 Thermal Evolution and EW Phase Transition

In this model, μ_s^2 is T -independent in the mean-field approximation ($c_s = 0$), while μ_h^2 and μ_1^3 depend on T in the usual way, now with $m_3 = \mu_m/12$. The evolution of the two curves $D_{h,s}^2(s)$ with temperature is then quite simple:

$$\frac{dD_h^2(s)}{dT^2} = -\frac{c_h}{\lambda_h}, \quad \frac{dD_s^2(s)}{dT^2} = -\frac{1}{3}. \quad (6.5)$$

As seen in the (h^2, s) -plane, when T increases, $D_{h,s}^2(s)$ shift towards the axis $h = 0$ without rotating. In order to have a proper cosmological evolution, starting in the symmetric vacuum at high T and ending up at $T = 0$ in the broken EW minimum, the line $D_h^2(s)$ should have slope smaller than that of $D_s^2(s)$ (this requires $8\lambda_h\mu_s^2 > \mu_m^2$) and it should move faster with T^2 than $D_s^2(s)$ (this requires $c_h > \lambda_h/3$, which is automatically satisfied). An example to illustrate this scenario is presented in Fig. 12. In the mean-field approximation the EWPhT

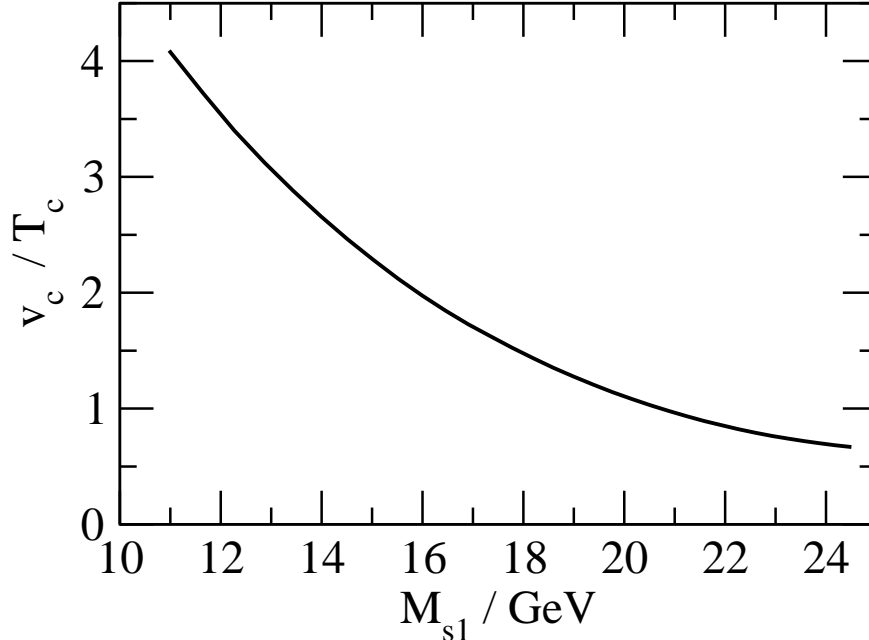


Figure 13: The ratio v_c/T_c in the scenario with a light scalar of Section 6 in the one-loop approximation as a function of the light scalar mass. Here $M_h \simeq M_{s2} \simeq 127$ GeV and $\mu_m = -40$ GeV.

would be second-order. However, a large $v(T_c)/T_c$ could be achieved after including in the potential the full one-loop corrections (that include a cubic term for h not only through transverse gauge bosons but also through the Higgs itself) if the model is tuned to have a nearly flat direction at T_c . The tuning involved, which we quantify by the small parameter $0 < \epsilon \ll 1$, requires nearly equal slopes for $D_{h,s}^2(s)$:

$$8\lambda_h\mu_s^2 = \mu_m^2(1 + \epsilon) = \epsilon_m^2(1 + \epsilon)v_{EW}^2 . \quad (6.6)$$

In terms of more physical parameters this reads

$$4M_h^2M_s^2 \simeq \epsilon_m^2 v_{EW}^4 , \quad (6.7)$$

which indeed requires a light scalar singlet, corresponding to the field excitations along the flat direction. Indeed, including the effects of s - h mixing, the two scalar mass eigenvalues are

$$M_{s1}^2 \simeq M_h^2 , \quad M_{s2}^2 \simeq \frac{1}{4}\epsilon_m^2 \epsilon \frac{v_{EW}^4}{M_h^2} . \quad (6.8)$$

Although it is difficult to imagine a symmetry reason that could lead to the relation (6.6), once that tuning is arranged, temperature corrections do not spoil it. In the mean-field

approximation the critical temperature is easily computed to be

$$T_c^2 = \frac{\lambda_h \epsilon v_{EW}^2}{c_h(1 + \epsilon) - \lambda_h/3}, \quad (6.9)$$

which shows that T_c can be made much smaller than in the SM, helping to increase $v(T_c)/T_c$. To determine this quantity one needs to carry out the one-loop analysis. Our renormalization conditions for this particular scenario are detailed in Appendix A. Fig. 13 shows our results. We have varied ϵ between 0.08 and 0.2, which roughly corresponds to light scalars with masses $M_{s_1} = 10 \div 25$ GeV, and we have fixed $\mu_m = -40$ GeV (this parameter has little influence on v_c/T_c) and $M_h = 120$ GeV (leading to $M_{s_2} \simeq 127$ GeV). We see that quite strong EWPhTs are possible, with v_c/T_c increasing with decreasing ϵ (or M_{s_1}), which makes the flat-direction flatter.

7 Numerical Examples. General Case

From the general analysis of the tree-level potential in Section 2 we have learned that the SM with a singlet has a very rich structure. In particular we showed in eqs. (2.37)-(2.40) that there are four distinct types of arranging for two degenerate minima in the potential, one of which, at (v, w) , breaks the electroweak symmetry while the other, at $(0, w_0)$, does not. The potential with these degenerate vacua is given by eq. (2.48).

7.1 Thermal Evolution and EW Phase Transition

As already explained in the particular cases studied in previous Sections, we take the previous potential with degenerate minima to hold at some critical temperature T_c and use the mean-field approximation to the free-energy to obtain the corresponding tree-level potential at $T = 0$. The temperature dependence of the potential parameters is very simple but finding how this dependence affects the minima, in particular $v(T)$ and $w(T)$, requires solving a cubic equation. A smart choice of the singlet shift can simplify this task by leading to simpler analytical expressions for these quantities. Here we simply perform this thermal evolution of parameters down to $T = 0$ numerically.

We start from one particular potential with degenerate minima, like those just discussed, expressed in terms of a set of original parameters $\{\mu_h^2, \mu_s^2, \mu_m, \mu_3, \mu_1^3, \lambda_h, \lambda_s, \lambda_m\}$. If we rescale all mass parameters by the appropriate power of some factor $A(T_c)$ we still have one potential with degenerate minima corresponding to the set

$$\{A(T_c)^2 \mu_h^2, A(T_c)^2 \mu_s^2, A(T_c) \mu_m, A(T_c) \mu_3, A(T_c)^3 \mu_1^3, \lambda_h, \lambda_s, \lambda_m\}. \quad (7.1)$$

case	M_{s1} / GeV	M_{s2} / GeV	$\sin(\alpha_{hs})$	λ_m	w / GeV	w_0 / GeV
a)	115.5	209.3	0.612	-0.1	600	120
b)	203.9	114.2	-0.429	-0.1	450	-90
c)	159.2	108.9	0.398	0.2	100	-520
d)	116.9	215.5	-0.621	0.15	130	676

Table 2: The parameters used in the general models of Fig. 14.

The thermally corrected potential (in mean-field approximation) for that rescaled potential reads

$$\begin{aligned}
V_T(h, s) = & -\frac{1}{2}A(T_c)^2\mu_h^2h^2 + \frac{1}{4}\lambda_h h^4 + \frac{1}{2}A(T_c)^2\mu_s^2s^2 + \frac{1}{4}\lambda_s s^4 + \frac{1}{4}A(T_c)\mu_m sh^2 + \frac{1}{4}\lambda_m s^2h^2 \\
& + A(T_c)^3\mu_1^3s + \frac{1}{3}A(T_c)\mu_3s^3 + \left[\frac{1}{2}c_h h^2 + \frac{1}{2}c_s s^2 + A(T_c)m_3s \right] (T^2 - T_c^2), \quad (7.2)
\end{aligned}$$

with c_h, c_s and m_3 as given in eq. (3.2). The factor $A(T_c)$ affects all dimensionful parameters and is used to guarantee $v(0) = v_{EW}$. The function $A(T_c)$ and the singlet vacuum expectation value at $T = 0$, w_{EW} , are obtained by solving numerically the minimization equations $\partial V_T/\partial h = 0$ and $\partial V_T/\partial s = 0$ at $T = 0$, $h = v_{EW}$, $s = w_{EW}$. Once $A(T_c)$ is known as a function of T_c , eq. (7.2) describes at $T = 0$ a family of potentials (parametrized by T_c) that lead to a strong electroweak phase transition.

Such potentials can be taken as the starting point for a full one-loop analysis of the EWPhT, including one-loop corrections at $T = 0$ and finite temperature, see Appendix A. We have performed such analysis for some representative families of potentials of the four different types discussed in Section 2. For our numerical examples we have chosen the parameters as given in Table 2, where α_{sh} is the scalar mixing angle. The results are presented in Fig. 14, which shows the ratio $v(T_c)/T_c$ as a function of T_c both in mean-field approximation (dashed line) and one-loop (solid line). The critical temperatures in both approximations differ and we also plot their ratio $T_{c,MF}/T_{c,1L}$ in the insets of each plot. Although the generic effect of including the full one-loop thermal corrections is always to increase the critical temperature and lower $v(T_c)/T_c$, Fig. 14 shows that very strong transitions can be obtained, with $v(T_c)/T_c > 1$ as required for successful baryogenesis, in all cases.

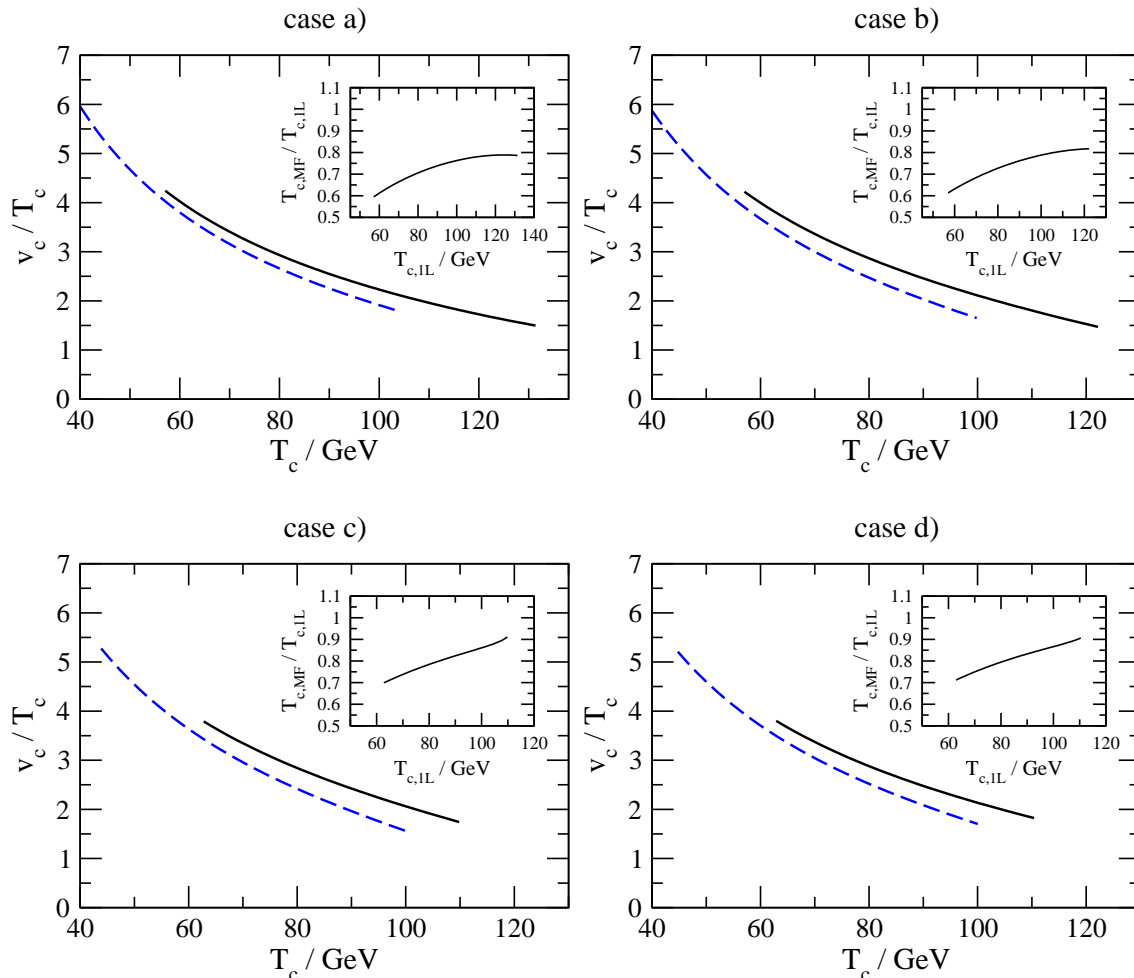


Figure 14: The ratio v_c/T_c in the mean-field approximation (blue dashed line) and the one-loop approximation (black solid line) as a function of the corresponding critical T_c for generic scenarios of different types, as indicated. The relation between critical temperatures in the two approximations is shown in the insets.

8 Conclusions

Our analysis of strong EWPhTs in the SM plus singlet highlights the richness of possibilities this simple extension of the SM offers. By relying on a simple mean-field approximation to the finite temperature scalar potential and a judicious choice of parametrization we have been able to perform a thorough analytical study of strong EWPhTs triggered by tree-level dynamics. We have given a strategy, summarized in Table 1, to identify the regions of parameter space that would lead to such strong EWPhTs. At the same time, our analytical approach has improved the understanding of the mechanisms behind such transitions allowing us to uncover new scenarios not appreciated before. One interesting example are

those transitions that rely on the presence of a flat direction in the potential at the critical temperature T_c , mechanism that could operate in many other models besides the SM plus singlet one.

We have computed the important ratio $v(T_c)/T_c$ both in particular realizations of the SM plus singlet model previously studied in the literature and in some representative examples of the most general model. In models with \mathbf{Z}_2 symmetry we have determined that a truly strong EWPhT based on a tree-level barrier must proceed from an EW symmetric vacuum that breaks the \mathbf{Z}_2 symmetry to an EW broken vacuum that is \mathbf{Z}_2 symmetric. In other particular models and in general, we have shown that $v(T_c)/T_c$ can be easily larger than 1. This is a necessary requirement for successful electroweak baryogenesis (switching off in the broken phase sphaleron processes that would erase the created baryon asymmetry). This jump in $v(T)$ is necessarily associated with a jump in the singlet VEV, which can also be relevant in some baryogenesis mechanisms. In addition such strong EWPhTs could also lead to a relic stochastic background of gravitational waves.

We have refined our analysis going beyond the mean-field approximation by including one-loop effects, with appropriate renormalization conditions at $T = 0$ and inclusion of thermal effects with daisy resummation and no high-temperature expansions. Although $v(T_c)/T_c$ is lowered by such refinement one still finds strong EWPhTs.

As a byproduct, our parametrization of the scalar potential of the SM plus singlet, which allows a good control over its vacuum structure, can be useful also at $T = 0$. In fact, the conditions summarized in the lower part of Table 1 can be applied at $T = 0$ to guarantee the stability of the EW vacuum and then our parametrization can be applied to phenomenological analyses allowing a direct control over physical quantities.

A Scalar Potential at Finite Temperature

One-Loop $T = 0$ Corrections

The analysis of thermal corrections to the scalar potential requires for consistency the inclusion of one-loop corrections to the potential at $T = 0$. These are given by the usual Coleman-Weinberg correction [50]

$$V_1(h, s) = \frac{1}{64\pi^2} \sum_{\alpha} N_{\alpha} M_{\alpha}^4(h, s) \left[\log \frac{M_{\alpha}^2(h, s)}{Q^2} - C_{\alpha} \right], \quad (\text{A.1})$$

where α runs over all degrees of freedom (counted by N_{α} , which includes a minus sign for fermions) with squared-masses $M_{\alpha}^2(h, s)$ (which depend on the scalar background fields h and s), C_{α} is a constant (equal to $3/2$ for scalars and fermions and to $5/6$ for gauge bosons) and Q is the renormalization scale, that can be fixed *e.g.* to the top mass. To this we add a counter-term potential

$$\delta V = -\frac{1}{2}\delta\mu_h^2 h^2 + \frac{1}{4}\delta\lambda_h h^4 + \frac{1}{2}\delta\mu_s^2 s^2 + \frac{1}{4}\delta\lambda_s s^4 + \frac{1}{4}\delta\mu_m s h^2 + \frac{1}{4}\delta\lambda_m s^2 h^2 + \delta\mu_1^3 s + \frac{1}{3}\delta\mu_3 s^3 + \delta V_0, \quad (\text{A.2})$$

specifically chosen so as to maintain the main properties of the tree-level potentials at $T = 0$ derived in the text. Those potentials have two minima, the one that breaks the electroweak symmetry at (v_{EW}, w_{EW}) and a symmetric minimum at $(0, w_{0,EW})$. The renormalization conditions we use cannot be used for potentials without this structure. In order to avoid problems with infrared divergent Goldstone contributions, we find convenient to remove the Goldstone corrections to V_1 in the renormalization conditions that follow (and we indicate this by writing \tilde{V}_1). This is simply a change of renormalization conditions and the shift it causes in the potential shape is negligible. For alternative treatments of this complication, see *e.g.* [51].

Explicitly, the renormalization conditions that we use are:

$$\left. \frac{\partial(\tilde{V}_1 + \delta V)}{\partial h} \right|_b = 0, \quad \left. \frac{\partial(\tilde{V}_1 + \delta V)}{\partial s} \right|_b = 0, \quad \left. \frac{\partial(\tilde{V}_1 + \delta V)}{\partial s} \right|_s = 0, \quad (\text{A.3})$$

(with the subindex b indicating evaluation at the broken minimum and the subindex s evaluation at the symmetric minimum) to ensure that the one-loop minima are still located at their tree-level positions;

$$\left. \frac{\partial^2(\tilde{V}_1 + \delta V)}{\partial h^2} \right|_b = 0, \quad \left. \frac{\partial^2(\tilde{V}_1 + \delta V)}{\partial h \partial s} \right|_b = 0, \quad \left. \frac{\partial^2(\tilde{V}_1 + \delta V)}{\partial s^2} \right|_b = 0, \quad (\text{A.4})$$

so that the tree-level mass matrix in the broken minimum is not affected at one-loop; then

$$\left. \frac{\partial^3(\tilde{V}_1 + \delta V)}{\partial s^3} \right|_b = 0, \quad (\text{A.5})$$

to have the same singlet cubic coupling; and finally

$$(\tilde{V}_1 + \delta V)|_b = 0, \quad (\tilde{V}_1 + \delta V)|_s = 0, \quad (\text{A.6})$$

so that the one-loop values of the potential at the minima are the same as the tree-level ones. These 9 conditions allow us to determine the 9 counterterms in δV as (dropping everywhere the subindex EW for simplicity)

$$\begin{aligned} \delta\mu_h^2 &= \frac{1}{2v^2} \left\{ \left[(3 - 5x_w^2)\partial_{h_r} - (1 - x_w^2)\partial_{h_r}^2 + x_w(3x_w - 2)\partial_{h_r s_r}^2 \right] \tilde{V}_1|_b \right. \\ &\quad \left. - 2x_w^2 \left(3\partial_{s_r} - \partial_{s_r}^2 + \frac{1}{6}\partial_{s_r}^3 \right) \tilde{V}_1|_b - 2x_w^2 \left(\partial_{s_r} \tilde{V}_1|_s - 4\Delta\tilde{V}_{1bs} \right) \right\}, \end{aligned} \quad (\text{A.7})$$

$$\begin{aligned} \delta\mu_s^2 &= -\frac{1}{2\Delta w^2} \left\{ (1 - 3x_w^2) \left[(5\partial_{h_r} - \partial_{h_r}^2)\tilde{V}_1|_b - 8\Delta\tilde{V}_{1bs} \right] + 2(1 - 6x_w^2)\partial_{s_r} \tilde{V}_1|_s \right. \\ &\quad \left. + \left[3(1 - 2x_w^2)(2\partial_{s_r} - \partial_{h_r s_r}^2) + \frac{1}{3}(1 - 6x_w + 6x_w^2)\partial_{s_r}^3 \right] \tilde{V}_1|_b \right\}, \end{aligned} \quad (\text{A.8})$$

$$\begin{aligned} \delta\mu_m &= -\frac{2}{v^2\Delta w} \left\{ \left[x_w \left(5\partial_{h_r} - \partial_{h_r}^2 + 9\partial_{s_r} - 2\partial_{s_r}^2 + \frac{1}{3}\partial_{s_r}^3 \right) + (1 - 3x_w)\partial_{h_r s_r}^2 \right] \tilde{V}_1|_b \right. \\ &\quad \left. + x_w \left(2\partial_{s_r} \tilde{V}_1|_s - 8\Delta\tilde{V}_{1bs} \right) \right\}, \end{aligned} \quad (\text{A.9})$$

$$\begin{aligned} \delta\mu_3 &= -\frac{3}{2\Delta w^3} \left\{ \left[x_w(5\partial_{h_r} - \partial_{h_r}^2 + 4\partial_{s_r}) + \frac{1}{3}(1 - 2x_w)\partial_{s_r}^3 \right] \tilde{V}_1|_b \right. \\ &\quad \left. - 2x_w \left(\partial_{s_r} \tilde{V}_1|_s + 4\Delta\tilde{V}_{1bs} \right) \right\}, \end{aligned} \quad (\text{A.10})$$

$$\begin{aligned} \delta\mu_1^3 &= \frac{3}{2\Delta w} \left\{ x_w \left[\frac{1}{4}(2 - x_w)\partial_{s_r} \tilde{V}_1|_s - 8(1 - x_w)\Delta\tilde{V}_{1bs} \right] + x_w(1 - x_w)(5\partial_{h_r} - 2\partial_{h_r}^2)\tilde{V}_1|_b \right. \\ &\quad \left. + \left[\frac{x_w}{3}(1 - x_w + 2x_w^2)\partial_{s_r}^3 + (1 - x_w)(1 - 2x_w)(\partial_{h_r s_r}^2 - 2\partial_{s_r}) \right] \tilde{V}_1|_b \right\}, \end{aligned} \quad (\text{A.11})$$

$$\delta\lambda_h = \frac{1}{v^3}(\partial_{h_r} - v\partial_{h_r}^2)\tilde{V}_1|_b, \quad (\text{A.12})$$

$$\delta\lambda_m = \frac{1}{v^2\Delta w^2} \left[\left(5\partial_{h_r} - \partial_{h_r}^2 - 3\partial_{h_r s_r}^2 + 6\partial_{s_r} - 2\partial_{s_r}^2 + \frac{1}{3}\partial_{s_r}^3 \right) \tilde{V}_1|_b + 2\partial_{s_r} \tilde{V}_1|_s - 8\Delta\tilde{V}_{1bs} \right], \quad (\text{A.13})$$

$$\delta\lambda_s = \frac{1}{2\Delta w^4} \left[\left(5\partial_{h_r} - \partial_{h_r}^2 - 2\partial_{h_r s_r}^2 + 6\partial_{s_r} - \frac{2}{3}\partial_{s_r}^3 \right) \tilde{V}_1|_b + 4\partial_{s_r} \tilde{V}_1|_s - 8\Delta\tilde{V}_{1bs} \right], \quad (\text{A.14})$$

$$\begin{aligned} \delta V_0 &= \frac{1}{3} \left\{ -2x_w^2 \left[(1 - x_w^2)\partial_{s_r} \tilde{V}_1|_s - 2(2 - x_w^2)\Delta\tilde{V}_{1bs} \right] - 4\tilde{V}_{1b} \right. \\ &\quad \left. + (1 - x_w)^2 \left[\frac{1}{2}(1 + x_w)^2(5\partial_{h_r} - \partial_{h_r}^2) + x_w(2 + x_w)(2\partial_{s_r} - \partial_{h_r s_r}^2) - \frac{1}{3}x_w^2\partial_{s_r}^3 \right] \tilde{V}_1|_b \right\}, \end{aligned} \quad (\text{A.15})$$

where $\Delta w \equiv w - w_0$, $x_w \equiv w/\Delta w$, $\Delta\tilde{V}_{1bs} \equiv \tilde{V}_{1b} - \tilde{V}_{1s}$ and $\partial_{h_r} \equiv v\partial/\partial h$, $\partial_{s_r} \equiv \Delta w\partial/\partial s$.

These counterterms have a finite $w \rightarrow 0$ limit, do not suffer from singularities (Δw cannot vanish), and do not spoil the \mathbf{Z}_2 symmetry when that is a symmetry of the Lagrangian. As explained in the text, strong transitions in this \mathbf{Z}_2 -symmetric scenario require $w = 0$. The form of the counterterms is much simpler in that case and can be obtained from the general formulas above simply setting to zero x_w and all odd s -derivatives of \tilde{V}_1 evaluated at the broken minimum. In particular, one gets $\delta\mu_m = \delta\mu_3 = \delta\mu_1^3 = 0$.

In the model discussed in Section 6 the tree-level potential does not have two degenerate minima but rather a nearly-flat direction, so that we do not use the previous prescription. In order to keep the nearly-flat structure at one-loop, we use instead the following renormalization conditions. For the broken minimum we impose that at one-loop it stays at the same tree-level location and with the same spectrum:

$$\left\{ \frac{\partial}{\partial h}, \frac{\partial}{\partial s}, \frac{\partial^2}{(\partial h)^2}, \frac{\partial^2}{\partial h \partial s}, \frac{\partial^2}{(\partial s)^2} \right\} (\tilde{V}_1 + \delta V) \Big|_b = 0 . \quad (\text{A.16})$$

The (tree-level) line $D_h^2(s)$ cuts $h = 0$ at $s = s_h$ and, to maintain this at one-loop we impose

$$\frac{\partial(\tilde{V}_1 + \delta V)}{\partial(h^2)} \Big|_{(0, s_h)} = 0 . \quad (\text{A.17})$$

Finally, the (tree-level) line $D_s^2(s)$ cuts $h = 0$ at $s = 0$ and, to maintain this and the same slope at one-loop we impose

$$\frac{\partial(\tilde{V}_1 + \delta V)}{\partial s} \Big|_0 = 0 , \quad 4\mu_s^2 \frac{\partial^2(\tilde{V}_1 + \delta V)}{\partial(h^2)\partial s} \Big|_0 = \mu_m \frac{\partial^2(\tilde{V}_1 + \delta V)}{(\partial s)^2} \Big|_0 \quad (\text{A.18})$$

where the subindex 0 indicates evaluation at $h = 0, s = 0$.

Finite Temperature Potential.

At the large temperatures of the early Universe plasma, high-temperature effects modify the Higgs effective potential (or rather, free-energy). The contribution of the different plasma species to the potential, in the non-interacting gas approximation, is given by standard one-loop (bosonic/fermionic) thermal integrals. Each particle species, labelled by α , contributes to the potential

$$\begin{aligned} \delta_\alpha V_T(h, s) &= \frac{T^4}{2\pi^2} N_\alpha \int_0^\infty dx x^2 \log \left[1 \pm e^{-\sqrt{x^2 + M_\alpha^2(h, s)}/T} \right] \\ &+ \frac{T}{12\pi} \delta_{\alpha b} N_\alpha \left[M_\alpha^3(h, s) - M_{T, \alpha}^3(h, s, T) \right] , \end{aligned} \quad (\text{A.19})$$

where $M_{T,\alpha}(h, s, T)$ is the thermally corrected mass of the corresponding species and the plus (minus) sign in the integrand is for fermions (bosons). The second line in (A.19) is present only for bosons (we represent this symbolically by writing δ_{ab}) and takes into account the effect of resumming hard-thermal loops for Matsubara zero modes. For our numerical work we used a series expansion of these integrals in terms of modified Bessel functions [26], avoiding high- T expansions.

The thermal masses in the SM plus singlet model are as in the Standard Model except for the scalar sector. The squared mass matrix for h and s is

$$\mathcal{M}^2 = \begin{bmatrix} -\mu_h^2 + 3\lambda_h h^2 + \frac{1}{2}(\mu_m + \lambda_m s)s & \frac{1}{2}(\mu_m + 2\lambda_m s)h \\ \frac{1}{2}(\mu_m + 2\lambda_m s)h & \mu_s^2 + 3\lambda_s s^2 + 2\mu_3 s + \frac{1}{2}\lambda_m h^2 \end{bmatrix} + \frac{1}{48} \begin{bmatrix} 9g^2 + 3g'^2 + 2(6h_t^2 + 12\lambda_h + \lambda_m) & 0 \\ 0 & 4(2\lambda_m + 3\lambda_s) \end{bmatrix} T^2. \quad (\text{A.20})$$

The thermally corrected mass for Goldstones is

$$m_G^2 = -\mu_h^2 + \lambda_h h^2 + \frac{1}{2}(\mu_m + \lambda_m s)s + \frac{1}{48} \left[9g^2 + 3g'^2 + 2(6h_t^2 + 12\lambda_h + \lambda_m) \right] T^2. \quad (\text{A.21})$$

Acknowledgments

J.R.E. and F.R. thank the CERN TH-Division for partial financial support and hospitality during the early stages of this work. We acknowledge support from the Spanish Ministry MICINN under contracts FPA2010-17747 and FPA2008-01430; the Spanish Consolider-Ingenio 2010 Programme CPAN (CSD2007-00042); and the Generalitat de Catalunya grant 2009SGR894.

References

- [1] M. C. Bento, O. Bertolami, R. Rosenfeld, L. Teodoro, Phys. Rev. **D62** (2000) 041302 [astro-ph/0003350].
- [2] C. P. Burgess, M. Pospelov, T. ter Veldhuis, Nucl. Phys. **B619** (2001) 709-728 [hep-ph/0011335].
- [3] J. McDonald, Phys. Rev. Lett. **88** (2002) 091304 [hep-ph/0106249].
- [4] H. Davoudiasl, R. Kitano, T. Li, H. Murayama, Phys. Lett. **B609** (2005) 117-123 [hep-ph/0405097].

- [5] A. Kusenko, Phys. Rev. Lett. **97** (2006) 241301 [hep-ph/0609081].
- [6] J. McDonald, Phys. Rev. **D50** (1994) 3637-3649 [hep-ph/0702143].
- [7] M. Gonderinger, Y. Li, H. Patel, M. J. Ramsey-Musolf, JHEP **1001** (2010) 053 [hep-ph/0910.3167].
- [8] P. Kumar and E. Ponton, [hep-ph/1107.1719].
- [9] Y. Chikashige, R. N. Mohapatra, R. D. Peccei, Phys. Rev. Lett. **45** (1980) 1926.
- [10] Y. Kondo, I. Umemura, K. Yamamoto, Phys. Lett. **B263** (1991) 93-96.
- [11] N. Sei, I. Umemura, K. Yamamoto, Phys. Lett. **B299** (1993) 286;
- [12] K. Enqvist, K. Kainulainen, I. Vilja, Nucl. Phys. **B403** (1993) 749
- [13] A. Riotto, Phys. Rev. **D49** (1994) 730 [hep-ph/9301235].
- [14] J. M. Cline, G. Laporte, H. Yamashita, S. Kraml, JHEP **0907** (2009) 040 [hep-ph/0905.2559].
- [15] S. J. Huber and M. G. Schmidt, Nucl. Phys. B **606** (2001) 183 [hep-ph/0003122].
- [16] A. Menon, D. E. Morrissey, C. E. M. Wagner, Phys. Rev. **D70** (2004) 035005 [hep-ph/0404184]; S. J. Huber, T. Konstandin, T. Prokopec, M. G. Schmidt, Nucl. Phys. **B757** (2006) 172-196 [hep-ph/0606298].
- [17] A. Datta, A. Raychaudhuri, S. Raychaudhuri, S. Chakrabarti, Z. Phys. **C72** (1996) 449 [hep-ph/9510432].
- [18] A. Datta, A. Raychaudhuri, Phys. Rev. **D57** (1998) 2940 [hep-ph/9708444].
- [19] R. Schabinger, J. D. Wells, Phys. Rev. **D72** (2005) 093007 [hep-ph/0509209].
- [20] D. O'Connell, M. J. Ramsey-Musolf, M. B. Wise, Phys. Rev. **D75** (2007) 037701 [hep-ph/0611014].
- [21] O. Bahat-Treidel, Y. Grossman, Y. Rozen, JHEP **0705** (2007) 022 [hep-ph/0611162].
- [22] V. Barger, P. Langacker, G. Shaughnessy, Phys. Rev. **D75** (2007) 055013 [hep-ph/0611239].
- [23] B. Gripiaios, A. Pomarol, F. Riva, J. Serra, JHEP **0904** (2009) 070 [hep-ph/0902.1483].

- [24] R. Barate *et al.* [LEP Working Group for Higgs boson searches and ALEPH Collaboration], Phys. Lett. B **565** (2003) 61 [hep-ex/0306033].
- [25] K. Kajantie, M. Laine, K. Rummukainen and M. E. Shaposhnikov, Phys. Rev. Lett. **77** (1996) 2887 [hep-ph/9605288]; Nucl. Phys. B **493** (1997) 413 [hep-lat/9612006].
- [26] G. W. Anderson and L. J. Hall, Phys. Rev. D **45** (1992) 2685.
- [27] J. R. Espinosa, M. Quiros, Phys. Lett. **B305** (1993) 98 [hep-ph/9301285].
- [28] J. Choi, R. R. Volkas, Phys. Lett. **B317** (1993) 385 [hep-ph/9308234].
- [29] J. McDonald, Phys. Lett. B **323** (1994) 339.
- [30] A. Ahriche, Phys. Rev. D **75** (2007) 083522 [hep-ph/0701192].
- [31] K. E. C. Benson, Phys. Rev. **D48** (1993) 2456.
- [32] S. W. Ham, Y. S. Jeong, S. K. Oh, J. Phys. G **G31** (2005) 857 [hep-ph/0411352].
- [33] J. R. Espinosa, M. Quiros, Phys. Rev. **D76** (2007) 076004 [hep-ph/0701145].
- [34] L. Vergara, Phys. Rev. D **55** (1997) 5248.
- [35] S. Profumo, M. J. Ramsey-Musolf, G. Shaughnessy, JHEP **0708** (2007) 010 [hep-ph/0705.2425].
- [36] A. De Simone, G. Nardini, M. Quiros and A. Riotto, [hep-ph/1107.4317].
- [37] V. Barger, P. Langacker, M. McCaskey, M. J. Ramsey-Musolf, G. Shaughnessy, Phys. Rev. **D77** (2008) 035005 [hep-ph/0706.4311].
- [38] A. Noble, M. Perelstein, Phys. Rev. **D78** (2008) 063518 [hep-ph/0711.3018].
- [39] J. R. Espinosa, T. Konstandin, J. M. No and M. Quiros, Phys. Rev. D **78** (2008) 123528 [hep-ph/0809.3215].
- [40] V. Barger, P. Langacker, M. McCaskey, M. Ramsey-Musolf, G. Shaughnessy, Phys. Rev. **D79** (2009) 015018 [hep-ph/0811.0393].
- [41] S. Das, P. J. Fox, A. Kumar and N. Weiner, JHEP **1011** (2010) 108 [hep-ph/0910.1262].
- [42] A. Ashoorioon and T. Konstandin, JHEP **0907** (2009) 086 [hep-ph/0904.0353].

- [43] R. Aureda, M. Maggiore, A. Nicolis and A. Riotto, Nucl. Phys. B **631** (2002) 342 [gr-qc/0107033]; A. Nicolis, Class. Quant. Grav. **21** (2004) L27 [gr-qc/0303084]; C. Grojean and G. Servant, Phys. Rev. D **75** (2007) 043507 [hep-ph/0607107]; S. J. Huber and T. Konstandin, JCAP **0805** (2008) 017 [hep-ph/0709.2091]; T. Kahniashvili, A. Kosowsky, G. Gogoberidze and Y. Maravin, Phys. Rev. D **78** (2008) 043003 [astro-ph/0806.0293].
- [44] S. Schael *et al.* [LEP Collaborations], Eur. Phys. J. C **47** (2006) 547, [hep-ex/0602042]; T. Aaltonen *et al.* [Tevatron Collaborations], [hep-ex/1103.3233]; and the latest bounds presented in the *Europhysics Conference on High-Energy Physics 2011* [<http://indico.in2p3.fr/conferenceDisplay.py?confId=5116>], in particular ATLAS-CONF-2011-112; CMS PAS HIG-11-011.
- [45] H. H. Patel and M. J. Ramsey-Musolf, JHEP **1107** (2011) 029 [hep-ph/1101.4665].
- [46] D. A. Kirzhnits and A. D. Linde, Annals Phys. **101** (1976) 195.
- [47] J. M. Moreno, D. H. Oaknin and M. Quiros, Nucl. Phys. B **483** (1997) 267 [hep-ph/9605387]; C. Grojean, G. Servant and J. D. Wells, Phys. Rev. D **71** (2005) 036001 [hep-ph/0407019].
- [48] M. Pietroni, Nucl. Phys. B **402** (1993) 27 [hep-ph/9207227].
- [49] C. Panagiotakopoulos, A. Pilaftsis, Phys. Rev. **D63** (2001) 055003 [hep-ph/0008268].
- [50] S. R. Coleman and E. J. Weinberg, Phys. Rev. D **7** (1973) 1888.
- [51] C. Delaunay, C. Grojean and J. D. Wells, JHEP **0804** (2008) 029 [hep-ph/0711.2511].